Characterisation of Truncated Mutant Rhodopsin and its Involvement in the Pathogenesis of Retinitis Pigmentosa

By Hannah N. M. Hargreaves

A thesis submitted for the degree of Master of science (by Dissertation) in Molecular Medicine

Department of Biological science

University of Essex

Date of submission (02.10.19)

Acknowledgements

I would like to thank my friends and family for all their support while completing this dissertation. I would also like to thank Philip Reeves my supervisor and Lynwen James my Lab technician for all their help and wisdom while completing this Masters. I would also like make a special mention to Chikwado alo Opefi for the use of his rhodopsin mutants.

Contents

Abstract

Autosomal dominant retinitis pigmentosa (ADRP) is the most common genetic disorders which cause visual degradation, and blindness. 20-25% of cases are caused by mutations in the rhodopsin gene. The mutations located in the N-terminus of rhodopsin produce severely misfolded protein, which has been shown to cleave at the N-terminus removing the glycosylation sites (Tam & Moritz, 2007), (Krebs, et al., 2010). We aimed to further understand the pathology of retinitis pigmentosa by separating full rhodopsin from the truncated rhodopsin of the mutant, and we constructed rhodopsin N-terminus ADRP mutations: T4K, P23A/H and Q28H. Wild Type and mutant rhodopsin were purified using 1D4-sepharose separation. Our results supported papers indicating P23A and T4K show lowest degrees of misfolding. Assuming the glycosylation sites are removed we attempted to isolate the truncated species of the ADRP mutant by Con A-Sepharose which binds to the glycan moieties extended from the glycosylation sites N2 and N15 (De Grip, W. J.,1982). We isolated purified ROS rhodopsin and full P23A rhodopsin. We failed to isolate the P23A truncated species, and poor binding was apparent from full rhodopsin in the wash and flow through after binding. Meaning the truncated species if present would not have been isolated. Further alterations are needed to make the Con A-sepharose separation successful.

Chapter 1) Literature review

1.1 The Structure of the Retina: with focus on the pathway of light and how this leads to vision.

The retina is a small plate of cells that lies at the back of the eye. It is 0.2 mm-0.5 mm thick and 30-40 mm in diameter and is comprised of central nervous tissue (Sung & Chuang, 2010) (Hubel, 2009)(Kolb, 2005). It consists of 6 main layers; retinal pigment epithelium ("RPE"), photoreceptors, horizontal cells, bipolar cells, amacrine cells, and ganglion cells. These cells/neurons together work to take a photon of light and convert it to a neuronal signal the brain can transform into a clear image of the world we see around us (Reminington, 2011). This system is very delicate and even the slightest alteration can cause a system failure.

The RPE is the cell layer that lies furthest from the point of light entry, followed by the photoreceptors which are so turned that the apical side faces the RPE (Sung & Chuang, 2010). The RPE is a monolayer of hexagonal cells, that forms part of the blood/ brain barrier (Strauss, 2005) and has many functions that are necessary for the visual pathway, these include: phagocytosis of POS (photoreceptors outer segment) in which 10% of volume is shed (Kevany & Pakczewski, 2012); the regeneration of 11-*cis*-retinal from all-trans-retinal; removal of excess and scattered light; protection of the retina from oxidative stress and is required for the removal and delivery of multiple ions and proteins.

To facilitate this transport and phagocytosis it has microvilli that extend from its apex membrane and wrap around the outer segment of photoreceptors. There are two types of microvilli; the longer microvilli are used for transport of glucose, retinol and fatty acids from the blood whereas the shorter microvilli form photoreceptor sheaths which help with phagocytosis of POS (Strauss, 2005). The essential products from the reaction, such as retinal, are recycled back to the photoreceptors for outer segment regeneration (Strauss, 2005). The RPE contains various pigments, including that of

melanin which is hypothesised to “mop up” any remaining light that is not absorbed by the photoreceptors, stopping the light from rebounding back. Providing a possible reason as to why the eye has developed in an inversed manner (Hubel, 2009). The RPE is also partly responsible for the regeneration of photoreceptors after bleaching (Strauss, 2005).

There are two types of photoreceptors, rods and cones. Rods mediate vision in dimly lit areas and in the periphery while cones are needed for bright light, and colour. Rod cells while highly sensitive have a low photon saturation, whereas cones are opposite in this respect (Kevany & Pakczewski, 2012). They are so called due to their shapes, while rods tend to be long and thin, cones are short and conical (Hubel, 2009). There are many more rods than cones with rods outnumbering cones 20 fold at about 130 million cells per retina (Sung & Chuang, 2010) (Masland, 2001). The rod cells are found in greater number towards the periphery of the cell however, the cones are found closer to the centre. The fovea, the central region of the retina where fine detail is best contains only cones which are densely packed. The fovea is central to vision and within this pit of the retina the light has a direct path from the pupil to the photoreceptor, as the other neurons have been pushed to the side (Hubel, 2009) (Sung & Chuang, 2010). This allows for a clearer, sharper, centre of vision. The main function of the photoreceptors is to absorb photons of light, via their opsin. Each photoreceptor has a different opsin, this protein in rod cells is named rhodopsin and will be discussed in below. This opsin once stimulated by the photon undergoes a process called phototransduction and sends a signal either to the bipolar cells or the horizontal cells.

In darkness photoreceptor cells are constantly secreting glutamate and only stop secretion once a photon of light has been absorbed and the cell has been stimulated. This constant secretion of the neurotransmitter means the horizontal cells are also stimulated at all times. Once the photon of light has been absorbed, the glutamate is no longer secreted causing the cell to hyperpolarise. There are two types of orizontal

cells, with two functions; to pass on the neuronal signal to bipolar cells, and lateral inhibition. Lateral inhibition occurs when the cell inhibits distant photoreceptors in its visual field to increase vision acuity (Masland, 2001) (Masland, 2012). The outcome is areas of light increase in brightness and areas of darkness become even darker leading to a clearer, sharper image (Thoreson, et al., 2008).

Bipolar cell dendrites synapse with photoreceptor terminals and horizontal cells (William, 2005), whilst its single axon synapses with ganglion cells and amacrine cells (Snell & Lemp, 1998). Bipolar cells have been classed on the basis of morphology, physiology, and dendritic contacts with photoreceptors, to reveal 12 types (Masland, 2012) (Reminington, 2011). Only one of these is a rod bipolar cell, the rod bipolar cell has a large cell body and several spike-like dendrites; these are the only bipolar cells which synapse with rod cells. As the retina evolved the rod photoreceptors also evolved transforming from cone photoreceptors leaving causing them to “piggyback” on the already ‘in place’ system (Masland, 2001). One rod bipolar cell’s dendrites can contact between 15-20 rod photoreceptors in the central retina and up to 80 rod photoreceptors in the periphery, thereby improving sensitivity. A rod bipolar cell interacts with more rod photoreceptors than a cone bipolar cells interacts with cone photoreceptors, meaning that more cone bipolar cells are required in the retina (Masland, 2001). This is seen in the case of invagination midget bipolar cells, which connect a signal cone cell to a single ganglion cell (Snell & Lemp, 1998) (William, 2005). The rod bipolar axon mainly contacts amacrine cells and very rarely contacts ganglion cells directly (Masland, 2001). This is to enable ganglion cells to carry information from both rod and cone cells (Reminington, 2011).

The ganglion cells have a diameter between 10-30 μm, and in most of the retina are a single layer. They are multipolar as their dendrites have the ability to synapse with both bipolar and amacrine cells. There are two types of ganglion cells: diffuse ganglion cells, and midget ganglion cells. The midget ganglion cell has one dendrite and

connects to either an invagination ganglion cell, or a flat midget ganglion cell, which might be linked to only one photoreceptor. This is likely to occur in the fovea where a single ganglion cell receives input from a single cone (Masland,2001) and again is used to enhance contrast detail and colour resolution (Reminington, 2011). Ganglion cell axons converge together at the optic disc to create the optic nerve. (William, 2005).

The photon of light passes from the photoreceptors through the pathway of neurons and finally to the ganglion cells which are present in the optic nerve, during this journey the light signal is converted to an electric signal which enables the brain to form an image of the world we see around us. The eye is one of the most complicated set of neurons found in the human body and one of the oldest, it is extremely sensitive to change, and failure of any of the neurons can lead to loss of vision.

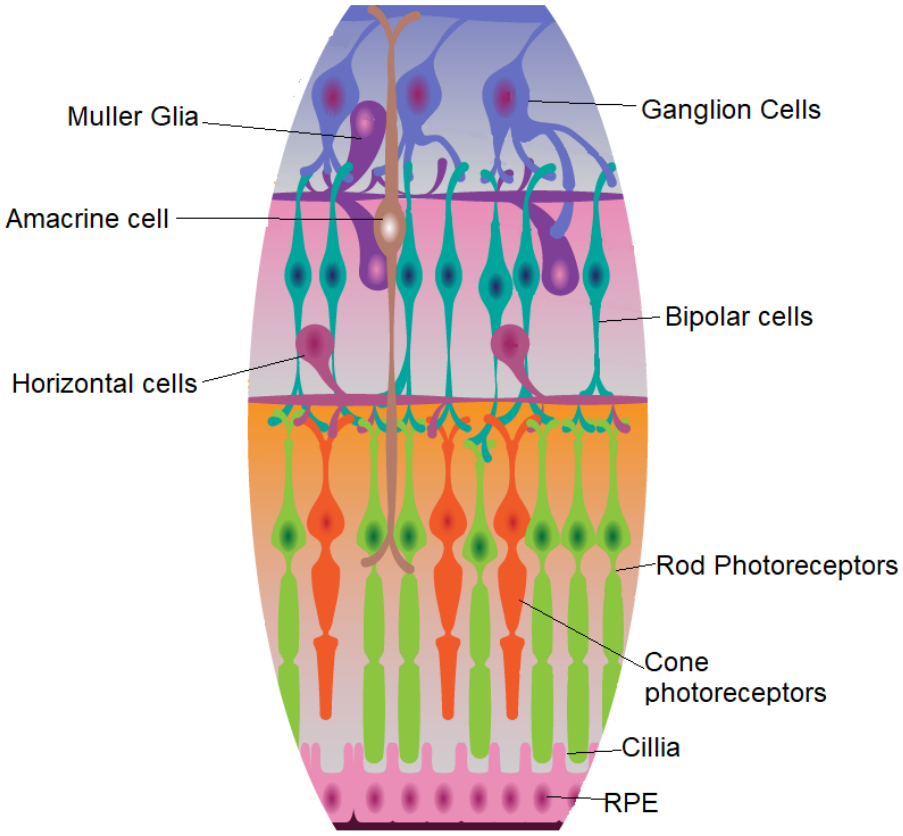

Figure 1 Basic structure of the mammalian retina. The diagram depicts the structure of the neurons and cells found within the retina. The Photon of light is absorbed by the photoreceptors, where, during photo transduction, it is turned into an electrical impulse. This impulse travels through the bipolar cells with the horizontal cells either acting as an indirect pathway or as a method to increase visual acuity. The impulse passes onto the ganglion cells, and to the brain where an image is formed. The amacrine cells again are used as an indirect pathway but have multiple different functions including inhibitory function. The muller Glia cells are used to aid functional and structural stability. This image was adapted from (LifeMap Sciences, 2019).

1.2 The structure of The Rod Photoreceptor with respect to movement of rhodopsin

Rod photoreceptors are highly sensitive and are needed for dim light conditions. There are 120 million rod cells in the human retina. The rod cells lie adjacent to the RPE and are vital for the survival of photoreceptors which are 40-60 µm long and 1.5-3 µm wide (William, 2005) (Molday & Moritz, 2015). The rod cells are long and thin in shape with a slight bulge in the cell body where the nucleus lies (William, 2005). It is formed of multiple sections; the outer segment (“OS”), the connecting cilium (“CC”), the inner segment (“IS”), cell body or nuclear region and the synaptic region or rod spherule.

The OS has a length of 30-60 µm and diameter 1.4-10 µm (depending on the species),and is filled with 600 - 1,000 flattened lamella shaped membrane discs (Sung & Chuang, 2010) (Reminington, 2011). Each of these discs are 2 µm in diameter, about 14 nm thick (Snell & Lemp, 1998), and are bridged by filamentous structures (Sung & Chuang, 2010). Rhodopsin, the GPCR photopigment, is incoporated into these discs upon their synthesis, at the base of the OS making up 95 % of the protein present (Sung & Chaung, 2010). The OS undergoes phagocytosis by the RPE in a removal and replacement cycle which lasts twenty four hours. Thus the rod cell is constantly sythesising new discs and new rhodopsin (Mcdevitt, 2012) (Kevany & Pakczewski, 2012). High density of rhodopsin, and ordered alignment with respect to light path, increases the probability of capturing a photon of light (Sung & Chuang, 2010).

The CC, connects the IS to the OS and allows for the passage of proteins (Molday & Moritz, 2015). Permitting them to run continuously through a narrow cylindrical stalk originating in the inner segment, it contains a modified cilium. This cilium has the standard nine double microtubule structure but lacks the central pair. The apical surface forms a ridge like structure that surrounds the CC circumference. The apical ridge is opposed to the basal OS (Sung & Chuang, 2010). Rhodopsin is trafficked to

the OS via the CC. It is believed rhodopsin has trafficking signals located on the c-terminus that help to direct the protein to the OS; this is a complicated system and its failure leads to many different retinal dystrophies (Nemet, et al., 2015). This trafficking of the rhodopsin molecule can be affected by the mutations that occur on the Rho gene. The trafficking system is very sensitive and relies on the correct folding of the protein so that it can be properly incorporated into the OS. The formation of poorly folded or misfolded proteins can lead to incorrect formation of the OS.

The IS can be thought of as comprised of two sections; ellipsoid and myoid. Ellipsoid is the closest to the OS and contains abundant mitochondria. Myoid contains the ER and the Golgi, and is the site of metabolism, biosynthesis, and endocytosis. The opsin which binds the chromophore to form rhodopsin is manufactured in the myoid of the inner segment before it is trafficked up and into the OS via the CC. The IS is connected to the cell body or nuclear region via the outer fibre which is about 1 µm wide (Reminington, 2011). The cell body contains the nucleus, which is the site of transcription. The inner fibre, contains many microtubules, it connects the cell body to the spherule (also known as the synaptic terminal) which contains the synaptic vesicles and synaptic ribbon (William, 2005). The rod spherules are the site of the synaptic contact between horizontal and bipolar cells (Li, et al., 2016) (Snell & Lemp, 1998) (William, 2005). This will be where the electrical signal is first fired to kick-start the process of vision.

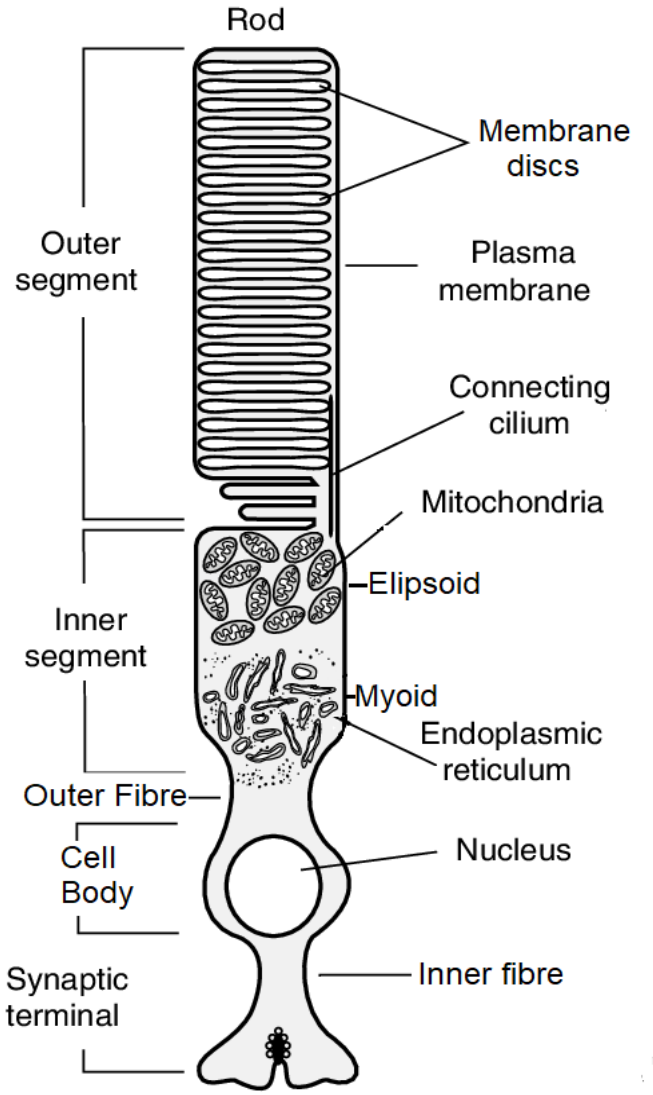

Figure 2 Basic structure of the mammalian rod photoreceptor. This is a schematic diagram of a rod photoreceptor fully annotated, showing the outer segment connected via the connecting cilium to the inner segment which allows for the trafficking of proteins. Clearly showing the difference between the two sections of IS; elipsoid containing only mitochondria closer to the OS and the Myoid which contains the ER and Golgi apparatus. This was adapted from (Cote, 2006).

1.3 The structure of rhodopsin with focus on the extracellular domain and the changes caused by activation.

Located in the OS, rhodopsin is the most abundant protein within the rod photoreceptor, responsible for scotopic vision, it is formed of opsin and 11-*cis*-retinal within the human retina. Rhodopsin is a GPCR, part of the A family. It is the best characterised GPCR that exists due to the easily accessible rhodopsin in bovines. Rhodopsin has the classic conserved 7 alpha helical transmembrane structure. However, unlike most GPCRs rhodopsin is constantly bound to its ligand 11-*cis*-retinal in both dark inactive states, and after phototransduction (Bourne & Meng, 2000). Rhodopsin functions to convert a light signal to an electrical signal, that can be used to form an image of the world around us, by absorbing a photon of light which triggers] the phototransduction cascade.

Rhodopsin is comprised of 348 amino acids and can be roughly distinguished by region: extracellular domain, intracellular domain, and membrane domain. The extracellular domain is composed of three extracellular loops (E1-E3), and the N-terminus, the intercellular domain is made up of three cytoplasmic loops (C1-3) and the C-terminus and the membrane domain is made up of 7α helices (Palczewski, et al., 2000).

The N-terminus consists of 5 distorted strands. The first two strands between the loci Gly^{3} to Pro^{12} are betta sheets and run parallel to the membrane. The other three strands form a right triangle between Phe^{13} to Pro^{34} with the third, strand 3 runs below the third extracellular loop, and the fourth strand connects Ser^{14} – Asn^{15} with Pro^{23} located close to the 1^{st} extracellular loop (Palczewski, et al., 2000). The oligosaccharide chains which extend from Asn^{2} and Ans^{15} attached during glycosylation do not have any interactions with rhodopsin and it has been suggested they could maintain orientation between E1 and N-terminal domains. Further evidence indicates the N-terminal domain remains static during activation, and that mutations

effecting glycosylation (T4K and T17M) have led to movement of this domain and thus instability of the protein. With one paper suggesting that the oligosaccharides may stabilise the molecule via steric hindrance and stabilising interactions (Tam, et al., 2014).

In the ground state 11-*cis*-retinal is bound at the Lys^{296} via a protonated Schiff base. The stability of this state is ensured by the Schiff base network which is made up of residues in the E2 loop, a hydrogen bond network, water molecules and the protonated Schiff base which forms a salt bridge with counterion Glu^{113} (Hofmann, et al., 2009). It is further stabilised by constraint tethers of TM3 and TM5 by a hydrogen bonding network which includes the use of Glu ^{222}, Trp^{126} and His^{211}. In large part Rhodopsin follows the general structure found in GPCRs with differences found in the ligand binding site, and the structural domain, designed to shield the hydrophobic retinal ligand from the aqueous phase (Hofmann, et al., 2009). The Ionic lock which stabilizes the inactive state is formed by the cytoplasmic network between E(D)RY motif on H3 and H6, which upon activation is removed (Vogel, et al., 2008). This Ionic lock includes Glu^{247} and Glu^{249} on H6, which are thought to form hydrogen bonds and ionic interactions with Glu^{134} and Arg^{135} on H3, and interhelical interactions with H7 (Vogel, et al., 2008) (Hofmann, et al., 2009) (Palczewski, et al., 2000). An additional structural motif present in inactive rhodopsin is NP xxY(X)F motif which is present on the TM7-H8 (Hofmann, et al., 2009).

Rhodopsin when subject to light undergoes a conformational change to active conformation, metarhodopsin II; it is in this conformation that rhodopsin binds G-protein transducin (Marin, et al., 2000). This leads to structural changes to the H6/H7 interface, the breakdown of the E(D)RY motif via protonation of Glu^{134} ,and the breakdown of the ionic lock and NP xxY(X)F motif, which allows formation of new interactions (Vogel, et al., 2008) (Hofmann, et al., 2009). Changes are found in TM5 which is extended by 1.5-2.5 helix turns and moves 2-3 A towards TM6. TM6 also

shows changes tilting outwards from the helix bundle by 6-7 A. These structural changes form a crevice in the cytoplasmic side of the receptor (Hofmann, et al., 2009). This crevice enables the binding of the transducin G protein.

It is known that the binding site for transducin is on the cytoplasmic surface, which has four loops, the fourth loop is bound to a helix only by its amino terminus. The charge pair Glu^{134}/Arg^{135}, conserved in all the G-coupled receptors, is required for binding transducin to metarhodopsin II (Khorana, 1992). Meta II decays to form either, apoprotein opsin, and all-trans-retinal or converts to a meta III by-product. Meta III has absorbance maximum 465 nm, and meta II an absorbance maximum of 380 nm. Meta III decays into free retinal and opsin, however interaction with Gt will enable it to form a meta II like species. Meta III can also serve as a storage for all trans-retinal, as it is toxic when free (Lomonosova, et al., 2012).

1.4 The Photo transduction cascade with emphasis on the importance of functional rhodopsin

Rhodopsin in the outer segment absorbs a photon of light, that causes the isomerization of 11-*cis*-retinal to all trans retinal, leading to a change in conformation state and thus activating rhodopsin. The activated rhodopsin interacts with the G protein transducin thereby catalysing the exchange of guanosine diphosphate.GDP for guanosine triphosphate GTP (Sung & Chuang, 2010). Transducin is made up of α, β and γ subunits, and is present along the membrane of the outer segment. This activation of transducin leads to the dissociation of α subunit GTP from the transducin and rhodopsin complex. The αGTP subunit activates the enzyme cyclic guanosine monophosphate cGMP- phosphodiesterase (PDE), which catalyses the hydrolysis of cGMP to 5'GMP. PDE is a peripheral protein which is tightly bound to an inhibitory protein in the dark; the αGTP subunit competes with this. This leads to a decrease in the concentration of cGMP levels, causing the cGMP gated channel to close, causing increased levels of calcium and sodium in the plasma. In response the cell hyperpolarizes, leading to a membrane potential of -75 mV (Reminington, 2011). Every rhodopsin activates at least 500 molecules of transducin, which each activate a PDE leading to the hydrolysis of 4,200 molecules of cGMP (Cox & Nelson, 2013).

To deactivate this membrane potential, the rhodopsin must be desensitised. Prolonged illumination of the rhodopsin protein leads to the exposure of Thr and Ser residues on the carboxyl-terminal domain, these residues are phosphorylated by rhodopsin kinase (Cox & Nelson, 2013). Rhodopsin kinase is not activated in the dark as the calcium binding protein, recoverin, binds to rhodopsin kinase when calcium levels in the cell are high. The re-coupling of the G trimeric protein occurs, the αGTP subunit has intrinsic GTPase activity, that can hydrolyse GTP back to GDP, causing the α subunit to dissociate from cGMP-PDE and re-associate with the trimeric protein transducin (Cox & Nelson, 2013). The rhodopsin protein binds with arrestin 1 which

prevents rhodopsin interacting with transducin. The lack of interaction with transducin causes a decrease in PDE activity, followed by the enzyme guanylyl cyclase being activated by GCAP and converting GTP to cGMP. GCAP is normally inhibited in the light by high calcium in the cell.

The all-trans-retinal is converted to all-trans-retinol in the outer segment. All-trans-retinal leaves the cell to the RPE to be converted back to 11-*cis*-retinal. The 11-c*is*-retinal is then transferred back to the photoreceptor to begin the cycle again (Sung & Chuang, 2010)

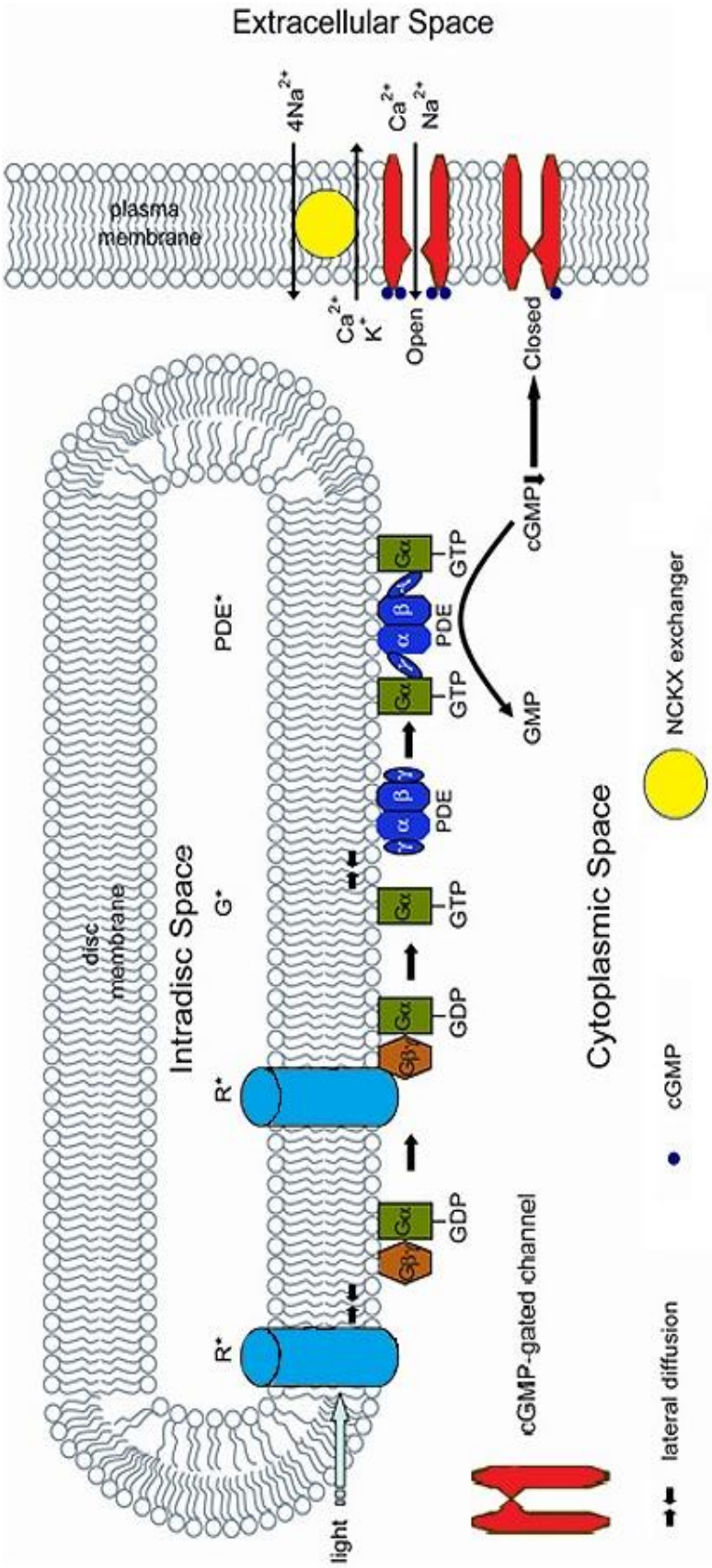

Figure 3 A schematic of the Phototransduction cascade. Once a light photon is absorbed by the rhodopsin it becomes activated starting the pathway, which enables a light signal to be converted into an electric impulse. The activated rhodopsin binds G protein transducin, leading to dissociation of αGTP. αGTP then binds PDE and converts cGMP into GMP causing a decrease of cGMP in the cell. This triggers hyperpolarisation of the membrane as a decrease of cGMP causes the gated channel to close. This figure was adapted from (Fu, 2018)

1.5 Introduction to retinitis pigmentosa its prevalence and Importance

Retinitis pigmentosa (RP) is the name given to a group of progressive degenerative inherited disorders, that target the rod photoreceptors in the retina and causes their death or non-function, eventually leading to degeneration of cone photoreceptors. (Hartlong, et al., 2006). Caused by multiple different mutations, the pathogenesis of the disease varies dependent upon the mutation type and the age of onset. Retinitis, meaning retinal inflammation, is a misleading term as it does not occur in RP and 'pigmentosa' referring to the melanin released by the RPE cells (Baumgartner, 1999). The name was originally coined by Dutch ophthalmologist F. C Donders in 1857 (Donders, 1857).

It is estimated that one in every four thousand of the world's population suffer from RP. It is the most common cause of inherited visual loss (Zhang, 2016) (Hartlong, et al., 2006) (Natarajan, 2011) (Verbakel, et al., 2018). It is the most common cause of inherited blindness with up to 25% of patients with RP become legally blind in both eyes (Natarajan, 2011) Research into the prevalence of non-syndromic RP in individual countries has shown no real difference based on location or ethnicity (Hamel, 2014). In Kuwait this disease was the leading cause of visual disability of individuals under the age of 60. In Denmark, RP and optic neuropathy were the leading causes of blindness in people aged 20-64 years, making up 29% of cases (Hartlong, et al., 2006). In Korea the overall prevalence is 1;9000 for all ages, increasing to a likelihood of 1:6000 for the over-40s. Korea also has higher mortality rates for those diagnosed with RP due to a high suicide rate among men of at working age (Na, et al., 2017). In Northern Ireland the rate is 1:3996 with a mean age of 50.4 years. (O'Neill, et al., 2007).

It is probable that late examination, bad diagnosis, and abnormal presentation can lead to misinterpretation of prevalence (Zhang, 2016). The impact of RP is far reaching affecting the individual, and those around them, including their children, spouses, and elderly parents. As Korea highlights it there are not just negative physical

consequences but also negative effects for mental health. It is imperative that a cure for the disease is found as soon as possible.

1.6 Onset and progression of retinitis pigmentosa; Diagnosis and current treatment

Retinitis pigmentosa progression can be influenced by many different factors including mutation type, age, gender, and general health. Pin-pointing the 'entry' age of onset is difficult and ranges from childhood to adulthood (Hartlong, et al., 2006). This is because RP is fundamentally heterogeneous with one paper showing that even among siblings the progression differs (Colombo, et al., 2018) (Daiger, et al., 2013).

The first symptom is night blindness, also known as nyctalopia (Ravichandran, et al., 2019), which can have late or early age onset although typically found in teenagers. However, it has been known to show in late 20s and early 30s. The earlier the age of onset the more sever the RP (Hamel, 2006). In most cases the most severe type of RP is caused by recessive mutants which typically have earlier onset and are more likely to cause total blindness. In its early stages RP may deliver peripheral visual field defects in dim light, however these are not apparent in the daytime. This symptom is not often caught when it first starts presenting as most people do not recognise it. This means the disease often progresses to cone damage before the sufferer seeks help (Hartlong, et al., 2006). It is believed that photoreceptor degeneration can start as early as 6, even in those who do not show symptoms until adulthood. The most effective means to diagnose RP this early is by the electroretinogram (EGR) (Hamel, 2006).

The sufferer loses peripheral vision, eventually developing tunnel vision, the age of onset once again varies between groups, sometimes dependent on the RP mutation type (Daiger, et al., 2013). Timings between stages is individual to each sufferer and some never reach blindness, or tunnel vision, and maintain only a mild form of RP. Patients can lose up to 90% of their cone cells before visual acuities start diminishing (Hartlong, et al., 2006). Ultimately in the worse instances RP progresses to loss of central vision, and most patients fulfil the legal definition of blindness by age 40

(Hartlong, et al., 2006). However this is not always the consequence of RP and in most dominant retinitis pigmentosa the sufferer never presents this final symptom.

There are three clinical findings which are indicate RP and thus are used as measures of diagnosis; bone spicule pigmentation, attenuation of retinal vessels, and optic nerve Pallor (O'Neal and Luther, 2019) (Ravichandran, et al., 2019). Bone spicule is caused by photoreceptor death which leads to a loss of pigment in the RPE, and a build-up of intraretinal melanin deposits (Athanasiou, et al., 2017), although bone spicule pigmentation is not apparent in all sufferers (Zhang, 2016).

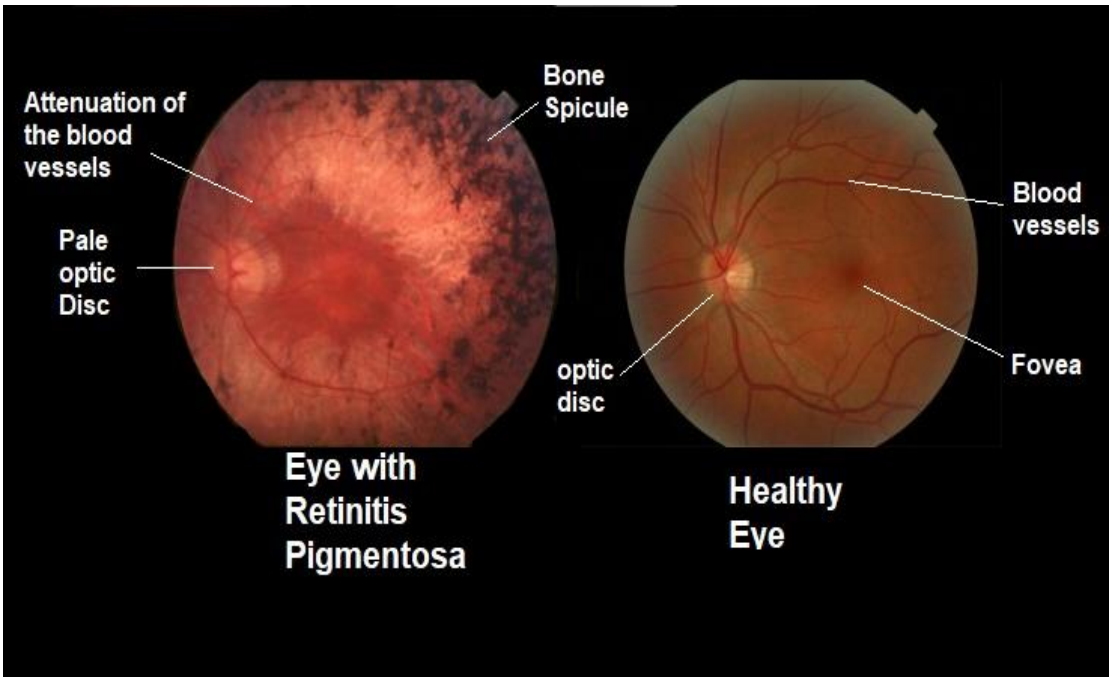

Figure 4 Labelled EGR images of a healthy eye, **(right) and an eye with retinitis pigmentosa (left).** This image highlights the different clinical findings used to diagnose RP ; attenuation of the blood vessels, pale optic disc, and bone spicule, all of which are not present [in]/[on] the healthy eye. This figure was adapted from (Schultz, 2013).

There is currently no cure for RP, but there are multiple treatments to slow progression. These include doses of vitamin A (no longer recommended as the relevant study was controversial (Natarajan, 2011)), light evasion, low vision aids, and more recently, more invasive methods such as Gene therapy, transplant research, and retinal prosthesis (Hamel, 2006). .

Currently there are experimental gene therapy tests ongoing for RP, these include; MERTK delivery in RCS rats and mice, RNA interference in animal model, and CNGB1 knock-out mouse model. Due to low transduction efficiency of recombinant gene vectors it has lacked long term benefits. Stem cell therapy using stem cells derived from bone marrow showed improvements within three months after treatment to quality of life for patients with RP but the effect was lost after twelve months (Zhang, 2016). For gene therapy to be most beneficial the mutation of each sufferer must be known, this makes testing, and improvements of the treatment, difficult.

While each of these therapies show varying degrees of success there is currently no universally accepted therapy.

1.5 Retinitis pigmentosa inheritance patterns with stress upon autosomal dominant RP

Retinitis pigmentosa accounts for half of all inherited retinal disease cases (Daiger, et al., 2013). The first gene responsible for RP was [discovered]/[found] in 1990 (Zhang, 2016) and the first mutation identified was P23H (Price, et al., 2011). Retinitis pigmentosa had been found to have nearly 3,100 mutations in more than 50 genes that cause non syndromic RP, more recently at least another 10 genes have been identified bringing the total to over 60 (Daiger, et al., 2019) There are three main forms of inheritance: Autosomal dominant which encompass 30-40% of cases, Autosomal recessive with 50-60% of cases. and X-linked with 5-15% of cases. These figures assume that isolated cases are recessive (Natarajan, 2011) (Zhang, 2016) (Hartlong, et al., 2006). These three types of inheritance normally affect different genes and thus have different mutations and pathogenesis, however in some cases overlapping genes which can fall under more than one type of inheritance. The rhodopsin gene, Rho accounts for 25% of ADRP cases, and 8-10% of all RP cases (Comitato, et al., 2016) (Price, et al., 2011).

RP is mainly non-syndromic however some 20-30% of RP cases show as part of a syndrome, and are categorised under 30 different syndromes (Hartlong, et al., 2006) (Zhang, 2016). The most common is Usher's syndrome which is associated with a hearing impediment and is apparent in 20-40% of recessive cases: 12 genes are known to cause Usher's syndrome (Hartlong, et al., 2006) (Daiger, et al., 2013). Other syndromes include Bardet-Biedl syndrome which has 17 genes linked [to]/[with] it, and is associated with obesity, renal disease, and cognitive impairment. These two syndromes alone account for 1,200 mutations clearly showing the heterogeneous of RP inheritance (Daiger, et al., 2013).

There are more than 150 documented missense/nonsense mutations on rhodopsin that cause autosomal dominant RP (Athanasiou, et al., 2017). 23 genes are known to

cause non-syndromic ADRP, 36 genes cause recessive, and 3 genes cause x linked RP, and around 20-25% of patients with ADRP have a mutation in rhodopsin (Hartlong, et al., 2006). The most common rhodopsin mutations are Pro23His and Pro347. The mutations of ADRP work in either a gain of function, or dominant-negative manner. The mutations found in rhodopsin are located all over the protein, those found in the cytoplasm tend to be more aggressive forms than those found in the extracellular space (Berson, et al., 2002). Interestingly the mutations located along the N-terminal have been linked to sector RP. Autosomal dominant is the mildest form with some sufferers not experiencing symptoms until age 50.

1.7 Different classifications of RP touching on their individual progression

A classification of the different types of mutants on the basis of pathology was introduced originally by Mendes and further reflected upon in other papers (Mendes, et al., 2005). In the original classification seven classes were found (Classes I, II, III, IV, V, VI, and VII), in subsequent papers these have been further compartmentalised and an class (VIII) has been added (Rakoczy, et al., 2011).

Class I mutations fold normally but have poor/no transport to the outer segment, due in part to the changes in the C-terminal caused by the mutations (Mendes, et al., 2005). Class II mutants are retained in the ER due to partial/misfolded rhod-opsins. During further assessment this class was divided into three sub-classes: Class IIa, Class IIb and Class IIc, sharing the following characteristics; destabilisation of the protein according to foldX, interference of the retinal binding area, and polar/charged residues interference with integration into the membrane and rhodopsin stability (Rakoczy, et al., 2011). Other changes to Class II include removal of T17M from class II to class IV due to glycosylation effects (Rakoczy, et al., 2011). P23H/A was classified as a Class IIa mutant. Class III: mutants effect endocytosis (Mendes, et al., 2005). Class IV have altered post translational modifications and affect stability of rod-opsin. T4K which was originally in this class has been moved to Class IVa (Rakoczy, et al., 2011). Class V show an increase in transducin activation. Class VI activate opsin without a chromophore and in the dark. The final class according to Mendes was just ‘unclassified’ showing no biochemical or cellular defect (Mendes, et al., 2005). Class VII is a new class of mutants which affect binding partner proteins, such as transducing or involve in dimerization of chromophore (Rakoczy, et al., 2011).

As previously stated, different mutants affect different genes, which in turn affect different proteins and thus different processes. One possible pathway for photoreceptor death is ER stress; accumulation of misfolded Class II mutants in the ER can lead to ER stress initiating UPR. In a normal process UPR can reduce the

number of misfolded proteins however if the stress is not elevated it can instead initiate apoptosis. Class II mutants can also be retro-translocated from the ER and undergo degradation by the ubiquitin-proteasome system (UPS), but if it is not degraded in this manner it can aggregate in the cytosol (Mendes, et al., 2005). Pharmacological chaperones is a possible therapy, especially of those class II mutants such as P23H. The hope is it will promote the trafficking and folding of these mutant rhodopsin, thus limiting the toxic effects of the mutants. AMPK activator metformin which alters cellular miliey and the rate of translation is another way to promote folding in mutated rhodopsin; however this leads to an unstable rhodopsin mutant (Athanasiou, et al., 2017)

1.8 The current understanding of the pathologies of the chosen N-terminal mutations

For the purposes of this experiment we are focusing only on the mutations located within the N-terminus of rhodopsin which are believed to cause Sector RP. As previously discussed, Sector RP only effects a segment of the retina and often leads to blindness in a specific location. These mutations are autosomal dominant, and while increasing the likelihood of presenting symptoms do not lead to severe symptoms such as full medical blindness. The mutations that we will be focusing on are; P23H, Q28H, P23A and T4K.

The N-terminal is of great interest because it is highly conserved. It is believed that mutations here can destabilise the protein by decoupling interactions of the cap with extracellular loops (Opefi, et al., 2013). The current belief is that these mutations lead to improper folding and inability to leave the ER. The ADRP mutants in the N-terminal such as P23H are some of the most common; P23H accounts for the largest fraction of ADRP mutations in the United States. (Opefi, et al., 2013). Many experiments on the mutations within the N-terminal have looked at 11-*cis* mediated pharmacological rescue as a means to treat the disease, 11-*cis* binds to rod opsin and is abundant throughout the cell, circulating the ER (Opefi, et al., 2013). It is thought that the pharmacological rescue of these mutated rhodopsins occurs naturally, allowing mutants to be transported to the OS, effectively going from a Class II mutant to a Class IV.

There has been evidence that while this occurs, the mutant is truncated via a protease in the ER, possibly to stabilise the rhodopsin. One study found a 28-Kda band on the P23H/L which was also seen at lower levels in P23A, T4R and T17M, this band has also been located in transgenic frog and mouse models (Tam & Moritz, 2007). The band is caused by a N-terminal truncated product of opsin that, under further observation was found to be a 2:1 mixture of two polypeptides, which were consistent with cleavage after Tyr29 and Pro23 (Krebs, et al., 2010). It is not known how this

mutant will be affected after interaction with light, although presumably, given the lack of N-cap, the rhodopsin will be unable to reform properly within the cell. It follows that these mutants would be sensitive to light, which is the case for T4K and T17M (Tam, et al., 2014), among other mutants that cause sector RP. For my thesis I have investigated the mutants T4K, P23H/A and Q28H, their location along the N-terminal produce different effects phenotypically, however they are all rescued in much the same manner.

T4K along with T17M sit on the N terminal close to glycosylation sites N2 and N15 (Zhang, 2016). The glycosylation of rhodopsin is believed to be critical to its ability to function. The glycosylation at N2 is not needed for the function of rhodopsin it is needed in N15 which is why the T17M is more toxic than T4K. There is also evidence that the toxicity of these mutants relies heavily on light, as they are less toxic in inactive and dark states. For conformational maturation and interaction with molecular chaperones rhodopsin requires N linked glycosylation in the ER (Tam, et al., 2014).

P23H mutation is much more severe than the P23A mutation, due to P23H having a more severely misfolded phenotype. The mutants T4R, T17M, and Pro23, all display unusual photobleaching behaviour. In the photochemical reaction pathway these show more metarhodopsin I like, and less metarhodopsin II like, characteristics immediately after illumination, implying that some molecules are converted into ground state, or into a isorhodopsin, during photobleaching. These intermediates are more light sensitive, and accumulation of these light sensitive decay products may be cytotoxic. Some of these variants may produce Intermediates which are unable to bind arrestin (Krebs, et al., 2010).

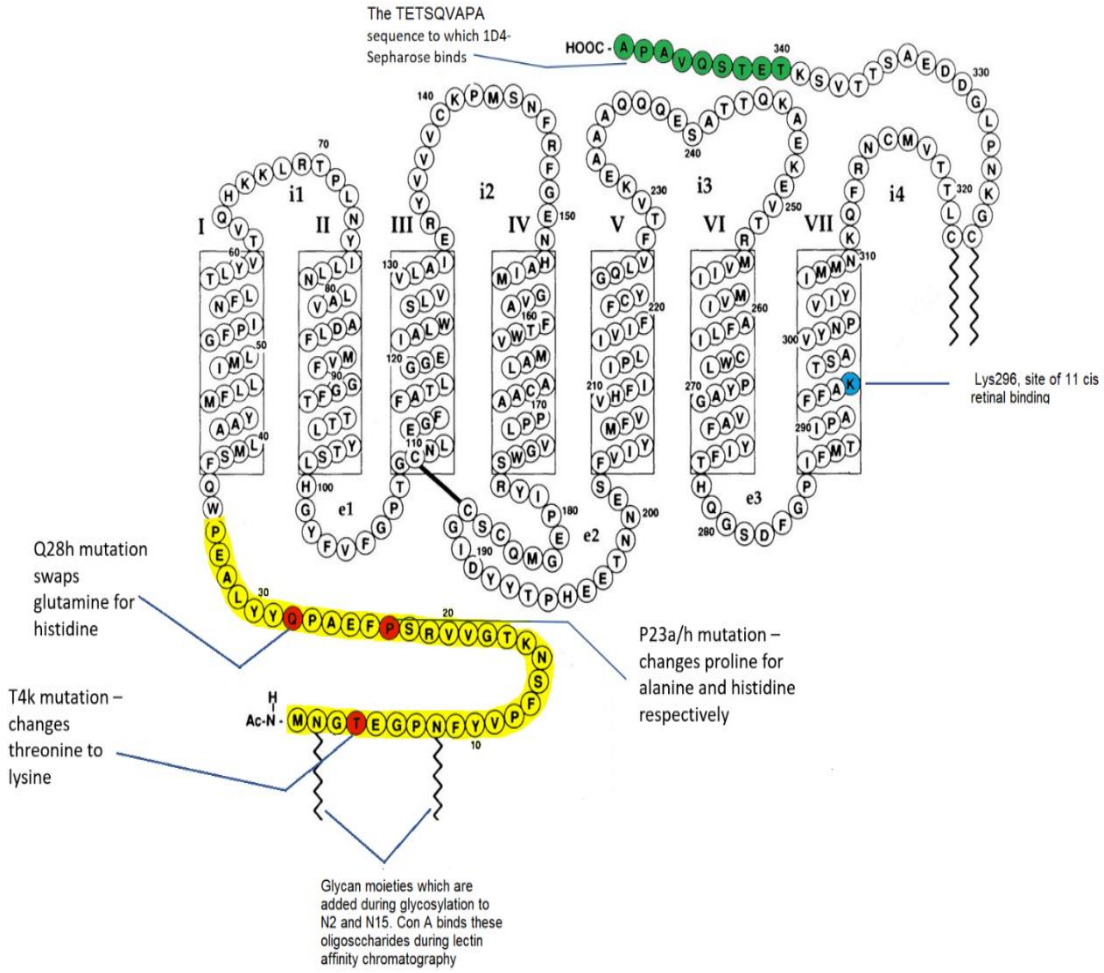

Figure 5 A schematic diagram of the secondary structure of rhodopsin. This image shows the location of the mutations on the N terminus (highlighted in yellow) that will be used during the experiments; T4K, P23H/A and Q28H (highlighted in red). This diagram also indicates the binding location of 1D4 Sepharose which is the TETSQVAPA sequence (highlighted in green) located on the C-terminus, and the location of binding for Con A – Sepharose which is the glycan moieties extending from N2 and N15 located on the N terminus of rhodopsin. The location of 11-*cis*-retinal binding has also been indicated at Lys 296 (highlighted in light blue). This figure was adapted from (Cha, et al., 2000).

1.9 Aims and hypothesis of thesis

The aim of this project was to express and isolate the cleaved rhodopsin and characterise it using biochemistry and spectroscopy, to see how it differs form the non-cleaved form. From this we hoped to increase understanding of the pathology of retinitis pigmentosa, this knowledge would help us to understand how the truncated rhodopsin causes retinitis pigmentosa, understanding its interactions with light and its ability to form intermediates such as metarhodopsin II.

We hypothesised that using two forms of immunoaffinity chromatography we could isolate the two mutant species. The first separation used 1D4-sepharose which binds at the C terminus to the TETSQVAPA sequence. The cleaved and full rhodopsin mutant species have functional a C terminus, thus we can use 1D4- sepharose as a way to purify the sample. The second separation uses Con A-Sepharose which binds to the glycan moieties extended from the glycosylation sites N2 and N15 (De Grip, W. J.,1982). Previous work has shown that the N terminus of the cleaved rhodopsin species is removed, this means it would be unable to bind to the Con A -Sepharose, allowing it to flow through. The full mutant rhodopsin species will bind to the Con-A sepharose thus isolating the two forms of rhodopsin.

If we can achieve this, we will then run photobleaching analysis and meta II rhodopsin decay analysis to better understand the characteristics of the ADRP rhodopsin mutant species. Once this species is isolated, we can use it to locate the kinase/kinases responsible for the truncation of rhodopsin.

Chapter 2) Methods

2.1 DNA Preparation

2.1.1 Formation of agar and broth

2xYT Agar:

- 16g/L of tryptone;
- 10g/L of yeast extract;
- 10g/L Na Cl;
- 16g/L agar.

Media was made up in RO water, aliquoted in 250ml sizes into 500ml Duran bottles, and autoclaved.

2xYT broth:

- 16g/L tryptone;
- 10g/L yeast extract;
- 10g/l NA Cl.

Media was made up in RO water, aliquoted into 3ml universal tubes, and autoclaved. All media was stored at room temperature.

2.1.2 Formation of agar plates

2xYT agar was warmed in a microwave until molten. The agar was left to cool to between 55°C and 40°C, and 100µg/ml filter sterilised ampicillin was added. The counter was sterilized with ethanol, and a bunsen burner lit in accordance with aseptic protocol. Agar was poured into 10cm petri dishes and left to dry in close proximity to the bunsen burner. The agar plates, once dry, were stored in the refrigerator for further use.

2.1.3 Generation of competent Escherichia coli cells

E. coli Cells previously prepared (Opefi, 2011) were used, Opefi's protocol is briefly outlined.

Transformation Buffer [(TB) (500ml)]:

HEPES (1.18g);

$Cacl_2$ (1.1g);

KCl (9.3g).

pH adjusted to 6.7 with 10M KOH

$Mncl_2$ (5.4g)

Final volume adjusted to 500ml.

TB was filter sterilized and stored at 4°C

Using a wire loop and aseptic conditions XL-1 Escherichia coli was struck out to single colonies on a non-ampicillin plate. A starter culture, made of a single colony suspended in 3ml 2xTY media without antibiotic selection, was grown over night (16hr) at 37°C on a shaker at 250rpm (New Brunswick Scientific Innova-4000). 100µl starter culture was inoculated into 250ml 2xYT media in a 2-L flask, which was incubated at 22°C with shaking at 200 rpm until the optical density of culture reached an absorbance of 0.6 at 600nm. Growth at 22°C was preformed was a refrigerated incubator shaker (New Brunswick Scientific Innova-4330), and 0.6 absorbance was attained by XL-1 blue cells within (26-30) h.

The cells were chilled on ice for 10 mins after growth, as well as all solutions. Cells were harvested by centrifugation (Jouan CR-312) at 400rpm at 4°C for 10 min. The pellet was resuspended carefully in 80ml of ice-cold buffer TB, re-centrifuged at 400 rpm at 4°C for 10 min. Supernatant was removed again, and the pellet suspended in 20ml ice-cold buffer TB. 1.5ml of high grade DMSO (sigma D-2650) was slowly added to the cells while swirling gently to ensure proper mixing. The cell suspension was

incubated on ice for 20min and aliquoted in 100µl or 200µl volumes into ice-chilled sterile 1.5ml tubes. The cells were snap frozen in liquid nitrogen and immediately stored at -80° C.

2.1.4 Transformation of E.coli cells

3µl of the DNA sample was added to 30µl of competent E.coli cells, left on ice for half an hour, and heat shocked for 45 seconds at 42ºC, before being immediately put on ice for 5 minutes. 500ul 2xty broth was added and put on a shaker at 250rpm for 30 mins at 37ºC-, (5mins on super coiled DNA). 50ul was pipetted onto each 2XTY plate containing ampicillin (100µg/ml) and spread; all completed under aseptic technique. The plates were then incubated at 37°c for 16 hours to allow colonies to form.

2.1.5 Construction of ADRP mutant genes

The plasmids used for this experiment were previously created for Chikwado Alo Opefim. They were constructed using QuickChange site directed mutagenesis.

2.1.6 DNA Sequencing

Sequence analysis was conducted out of house by SourceBiosciences. They were sequenced backwards and forwards in the case of the TETO plasmids, and the other mutants were tested normally.

2.1.7 Mini-scale DNA preparation

The mutant or WT plasmid DNA was grown on ampicillin plates; one colony was selected from each plate and inoculated in 3ml of 2xty broth with ampicillin, again at 100 mg/ml, and left on a shaker for 16 hours (or over-night) at 37°C. 1 ml of the culture was inoculated into a microcentrifuge tube and spun at maximum speed for 3 minutes at RT. The suspension was removed, and the pellet prepared using the Thermo Fisher Scientific Mini-prep kit (Fisher,2019). The elution buffer was replaced with miliQ water at 65°C; 500 µl was used. The concentration and quality of the DNA was measured using a nanodrop spectrometer. The sample was kept at-20°C until used.

2.1.8 Midi –scale DNA preparation

Plasmid DNA was grown on ampicillin plates and the culture left to grow over-night. A single colony was selected and inoculated in 2XTY broth with ampicillin at 100mg/ ml. The suspension was put on a shaker for 6-7 hours at 250RPM at 37°C. An aliquot of this was inoculated into a 1 L conical flask of 2xty broth (100 ml), again with ampicillin at 100 mg/ml. The broth was left on the shaker over- night at 37°C at 200RPM. The broth was removed and divided into two 50ml centrifuge tubes centrifuged at 4,500 rpm for 5 mins at RT. The pellet was kept at -20°C until use. The pellet was prepared using the Thermo Fisher Midi Prep kit (Fisher, 2019). The DNA was eluted, and the concentration tested as in 2.1.7.

2.2 Tissue cell culture

The cells used in this investigation are human embryonic kidney 293s cells which were previously stored in cryogenic tubes at -80°C. The cells were grown under sterile conditions in a tissue culture laboratory. The cabinet used was a class II type A2 biological safety tissue culture hood (sanyo NU-427-400) equipped with vertical laminar flow and UV light for decontamination. PPE was worn where appropriate.

2.2.1 Tissue cell culture media

Full DMEM, and DMEM F12, were supplemented with; 1% penicillin streptomycin, 10% foetal bovine serum, and 1% stable glutamine.

The media and its supplements were warmed to 37°C and mixed together in a tissue culture cabinet under sterile conditions. All media was stored at -20°C

2.2.2 Growing stocks from frozen

HEK 293s cells, and supplemented DMEMF12, were warmed to 37°C in a water bath and washed with 70% ethanol before being moved to a tissue culture lab where they were disinfected using 2% chem gene in accordance with aseptic technique. The cells were added to a 15 ml centrifuge tube, and 10 ml supplemented DMEMF12 was added drop wise. The cells were centrifuged at 1,000 RPM for 3 minutes at RT. The supernatant was removed, and 10 ml of supplemented DMEMF12 was used to resuspend the cell pellet. The suspension was added to a 10 cm TC plate which was incubated at 37°C with 5% $C0_2$.

2.2.3 Sub culture and splitting cells

10 cm plate

When cells reached 90% confluence they were divided, every two days thereafter the cells were further divided at a 1:4/ 1:5 ratio. PBS, supplemented DMEM F12 and trypsin were prewarmed to 37°C, in a warming cabinet. The plate was removed from the incubator to a pre-disinfected TC hood. The old media was removed using an

aspirator containing chem gene at 5%. The cells were washed with 10 ml PBS and then aspirated off; 1 ml of trypsin was added, and the plate placed in an incubator for 2mins. 8ml media was added to two new plates, and 7.5 ml added to two other new plates for a 1:5 and 1:4 split. The original plate was removed and the trypsin inactivated by 9ml of media. The media was pipetted up and down the plate to remove all cells and assure a 1 cell suspension. 2 ml of this media was added to the 8 ml plates, and 2.5 ml added to the 7.5 ml plates. The plates were then moved from side to side to achieve full coverage of the plate and avoid grouping. The plates were to an incubator at 37°C with 5% $C0_2$.

15 cm plate

As for the 10 cm plate, except with 15 ml PBS and 2 ml of trypsin. A previously autoclaved 250 ml duran bottle was filled with 65 ml of supplemented DMEMF12 media. The plate was removed from the incubator and 8 ml of media added, then pipetted to get a single cell suspension. The media was added to the 250 ml duran bottle, then swirled. 18 ml of this media was distributed via a pipette to the four plates. The method then followed that for the 10 cm plate.

2.2.4 Freeze down

When the HEK 293s cells achieved 90% confluence the media was aspirated, the plate was washed with pre-heated PBS and either 1 or 2 ml of pre-heated trypsin added, the plate was incubated at 37°c and 5%$C0_2$ for 2 minutes. The trypsin was inhibited by the addition of 8 or 9 ml of pre-heated supplemented DMEMF12, the suspension pipetted up and down ten times to ensure single cell suspension. The suspension was transferred to a 15 cm tube, and spun at 1,000 rpm for 3 minutes at RT. The supernatant was removed, and the pellet re-suspended in 10 cm freezing serum (90% supplemented DMEM :10% DMSO). The suspension was aliquoted into freezing vials for storage at -80°c.

2.2.5 Preparation of 9 cis retinal

Stock Solutions

Stock solutions of 10 mM were made using 25 mg 9 cis-retinal (Sigma R5754:514-85-2). The 9 cis was dissolved in ethanol, added to a 15 ml tube and left to rock until dissolved. The stock solution was aliquoted into freezing vials and sealed with Argon, the vials were wrapped with foil before being stored at -80°c.

Working solutions

An aliquot of stock solution was removed and aliquoted further for final concentration of 20 µM. The retinal solution underwent evaporation of ethanol by argon, and subsequent re-suspension in cell culture grade DMSO.

2.2.6 Transient transfection of mutant rhodopsin

The HEK 293s cells were grown in supplemented DMEMF12 until confluent and then split for 35-40% confluence in complete DMEM. Transfection was completed using the $CaCl_2$ method as previously denoted, briefly per 10 cm plate; 27 µg Rho-pMT4 DNA, and 3 µg pRSV-Tag DNA, were made up to 450µl milliQ water in a 15 cm tube. 2.5 M $CaCl_2$ was added drop wise to the solution under constant vortexing followed by 2X BES buffer which was added drop wise under time constraints. This 1 ml solution was added gently drop wise to the plate of HEK 293s cells while being briefly swirled. The cells were incubated overnight at 37°c and 1% $C0_2$. The old media was removed and the cells washed using PBS, new media was added and the cells incubated at 37°C and 5% $C0_2$ for 48 hours. The cells were harvested and pelleted down, the supernatant removed, and the pellet re- suspended in 1.5 ml PBS. The 2 µl 9-*cis*-retinal from stock was added to cell suspension and, in dark conditions incubated at -20°C for 3 hours in a nutator. Thereafter the cells were wrapped in foil, snap frozen, and stored at -80°C.

2.2.7 Transfection with retinal rescue

The transfection solutions were added as described above and left for 24 hours. The transfection solutions were removed, the cells washed, and new media added. The cells were subsequently rested in an incubator at 37°c and 5% $C0_2$ for approximately six hours. The 20 µM 9-*cis*-retinal previously prepared in methods section 2.2.5and under dark light and sterile conditions was added drop wise to the plates. The plates were gently swirled before being wrapped in foil and placed back in the incubator at 37°c and 5% $C0_2$. The procedure then follows the methods described in section 2.2.6.

2.2.8 Stable cell line transfection of mutant rhodopsin

Plasmids, suitable for use in creating a stable cell line, were grown from frozen following procedures described in section 2.1 and more specifically: 2.1.2 to 2.1.4 and 2.1.6. The plasmids were created as previously described in (Reeves, et al., 2002) but briefly the plasmid contains two TETO sequences (tetracycline-inducible expression system) attached to a CMV promoter, the acetylcholine esterase Ach(nc) gene and the rhodopsin gene, creating the pACMV-tetO-Rho plasmid. This plasmid was mutated so that it produced either P23H or P23A rhodopsin.

The HEK293S cells used in the experiment were previously transfected with the pCDNA6-TR (Invitrogen) plasmid containing genes encoding the selectable marker blasticidin and the tet operon repressor protein (TetR). The cells were brought up from frozen (as previously described in methods section 2.2.2) and were selected based on basticidin (5µg/ml) resistance. Those cells showing resistance were expanded under blasticidin selection and transfected with plasmid pACMV-tetO-Rho using the calcium method described in method 2.2.6. After 48 hours geneticin (2 mg/ml) selection was initiated, and colonies appearing after 14 days were isolated and expanded on a 24 well plate. The cell lines were divided1:3 down the lanes. The first well was frozen and stored at -80°C, the second well supplemented with growth medium, and the 3rd dish

induced using tetracycline (2 µg/ml) and sodium butyrate (5mM). The wells were left for a further 24 hours, harvested, and frozen at -80°C.

2.3 Protein purification

All purification and separation procedures were carried out in the dark or under safelight filter and at 4°C

2.3.1 Purification of mutant rhodopsin via rho-1D4-Sepharose beads

Purifications started with original samples of WT between 80-100 µg, and mutant types between 40-60 µg, as calculated from the UV Spectra (2.4.2) of the harvested transiently transfected rescued cells (2.2.6).

Buffer A – solubilisation buffer

0.1% DDM;

0.5 mM PMSF;

made up in 1x PBS.

Buffer B – Wash Buffer

Buffer A – without PMSF

Buffer C – Elution Buffer

Buffer B + 100 µM Rho-1D4 peptide

The sample was brought to 2 ml in buffer A and, in the dark, rotated for an hour at 4°C before centrifugation at 4,500RPM at 4°C for 30 minutes. 50% of 1D4 slurry (Amersham Pharmacia previously prepared in 50% slurry in PBS) was added to the sample and left, in the dark, to rotate at 4°C for a further 2 hours. The suspension was loaded into a disposable polypropylene column (Thermo Scientific 29920) equipped with a porous disc (frit) and capped. The column was suspended over a 100 ml measuring cylinder. 10 ml of buffer B was added to the column, then another. The column was capped and incubated overnight at 4°C overnight. The wash buffer was allowed to flow through the column before100 µl of buffer C was added and also allowed to flow through. The column is capped and a further 500µl of buffer C was

added to the column, the column was incubated for an hour at 4°C. The column was then uncapped and the flow through collected in a second centrifuge tube. The process of adding 500 µl of buffer C and incubation for an hour at 4°C was repeated a further 3 times. The UV spectra was then taken.

2.3.2 Protein Purification using CON A- Sepharose beads

Buffer A – Solubilisation Buff

0.01M $CaCl_{2;}$

0.01M MnCl2;

0.05M NaCl2;

0.01% DDM;

made up in 1% PBS

Buffer B – Wash Buffer

Buffer A made up in 7.6 pH Tris HCl

Buffer C – Elution buffer

Buffer B + 0.3 M of Methyl α-D-Mannopyranoside

The centrifuge spin columns were prepared, and 0.03 ml of Con A beads in slurry were added to it. The column was washed 10 x with 250 ul of buffer B. A small aliquot of the Sample was removed for Western blot analysis, the remainder of the sample was made up to 1.5 ml in buffer A. The Sample was rotated for an hour at 4°C before centrifugation for 30 mins at 14,000 RPM at 4°C. The pre-prepared spin column was transferred to a fresh 1.5 ml centrifuge tube, and the Sample added to the spin column. The centrifuge tube containing the spin column was rotated for two and one half hours at 4°C using a mini centrifuge, and a UV spectra taken to confirm full binding. The spin column was transferred to a fresh centrifuge tube and 500 µl buffer B was added, the column spun down again and another UV spectra taken. Thereafter the column was

transferred to a fresh centrifuge tube, 500µl buffer C was added to the column, which was rotated for a further hour at 4°C, the column was again spun down and again a UV spectra taken. This was repeated for a number of elution fractions until all rhodopsin had been collected.

2.4 Analysis of samples

2.4.1 Western blots and SDS page analysis

See appendix section 1.1 for buffers.

Glass slides were washed in succession with 1% SDS, 70% ethanol, and RO water. The gel rig was assembled according to the manufacturers' instructions. The resolving gel solution was made up, loaded into the gel rig, and overlayed with 0.5 ml of water-saturated iso-butanol.

The running gel (appendix section 1.1 Table 1 referred), was left to polymerise and washed thoroughly with RO water, and dried using blotting paper. The stacking gel (appendix 1.1 Table 2 referred), was loaded and the 10 well comb was then added immediately, and the gel left to polymerise.

The gel cassettes were placed into the clamping frame as per the manufactures' instructions. The electrode assembly was placed in the buffer tank, and 1x tank buffer was added to the assembly just under the gel plate. The comb was removed and the gels syringed with 1X tank buffer, this was left so leaking could be monitored. The samples were prepared; separately 64 µl of 4x loading buffer was added to 16 µl of mercapethanol, and 4 µl of this solution was added to 12 µl of the samples. The ladder was also prepared using 1x loading buffer and a prestained protein page ruler, product number 26616. The samples were added to the wells, with a detailed note of the order being was made. The Hoefer ps300-B power pack was attached and set at 200V initially for an hour and additional time added as necessary to ensure the dye had travelled down the gels. Transfer buffer was added to a clean tray, and four blotting papers of the correct size were submerged together with a membrane, the sponges, and the clamp. The gels were then removed and one placed in coumassie stain and left on a rotator for an hour, another was submerged into the transfer buffer. The clamp was assembled according to manufacturers' instructions in the order: one sponge, two

blotting papers, the membrane, the gel, two further blotting papers, and another sponge; any air bubbles were rolled out gently before the clamp was tightened. The clamp was then added to the assembly, in accordance with the manufacturers instruction, with the addition of a magnetic stirrer, an ice pack and the assembly being placed in an ice bucket to keep temperatures down. The power back was set to 100v for an hour, thereafter the membrane was removed to the blocking buffer and left overnight on a nutator at 4°C. The coumassie stain gel was removed from the rotator and kept overnight at 4°C, before a photograph was taken of the gel. The western blot membrane was washed with 1x PBS, primary antibody was added and left on a nutator for 5 hours, washed using the wash buffer 5x for 5 minutes, secondary antibody is added for one hour and washed a further 5x with the wash buffer, finally the ECL was added and incubated at RT for 1 min. The membrane is then wrapped gently in cling film and attached to the detection chamber of a radiographic cassette. The remainder is performed under dark conditions: a photographic film is exposed to the membrane for 10-60 seconds, the film is placed briefly in a developer, washed in RO water, and then submerged in a fixer solution for 10 minutes before being washed again with RO water. The film is then left to dry.

2.4.2 UV spectroscopy

Appendix section 1.2 for buffers referred.

UV visible spectroscopy was taken using the Perkin-Elmer λ25 UV/vis spectrophotometer equipped with water-jacketed cell holder. The room and water jacketed cell holder were at 19 °C, with the samples being kept in dark conditions at 4°C. The data interval was set at 2 nm bandwidth with a response time of 1 sec and a scan speed of 480 nm/min, and spectral scans taken between 650 nm and 250 nm wavelengths. The samples were analysed using UV spectroscopy include; samples of transiently transfected harvested cells solubilised in DDM (2.2.4), multiple stages of 1D4-sepharose purification in section 2.3.1, and multiple stages of CON-A – sepharose separation in section 2.3.2. Blanks were made up of the buffer in which the sample had been solubilised. The inside of the curvet was cleaned using 1% DDM, RO water and 100% ethanol in that order, and the outside cleaned using non scratch wipes.

An aliquot of the samples of harvested cells in section 2.2.4 was made up to 500 µl in buffer A, mixed end over end in the dark for 1 hour at 4°C, and centrifuged for 30 mins at maximum speed at 4°C. The blanks were made up using buffer A and the spectroscopy machine was prepared. Each sample was then measured under dark conditions before photobleaching for 60 seconds using a fibre optic guide directly to the curvet, and the UV spectra was re-checked. The samples were saved for western blot analysis. The two UV/Vis spectra were then compared, the bleached sample was zeroed to the dark spectra, and the zeroed bleached spectra was subtracted from the dark spectra to create the difference spectra, which was used to calculate the amount of rhodopsin present in the sample.

The blanks for the stages of the purification and separation protocol can be found in section 2.3

2.4.3 Dot blots

Appendix section 1.3 for buffers referred.

Transiently rescued T4K sample, previously analysed by western blot, was used as a positive control, and untransfected harvested cells, previously analysed by western blot, were used as a negative control. The stable cell line pellets were re-suspended/ solubilised in buffer A. The samples were mixed end over end at 4°C for an hour and centrifuged at maximum speed for 30mins at 4°C. The dot blot apparatus, 96-well Bio-Dot®, was assembled according to manufacturers' instructions, appendix section referred. Samples were prepared in the 96 well plate. 75 µl of buffer B was added to each well using a multichannel pipette. 25 µl of each sample was added to the first row, using the multichannel pipette. 25 ul of the first row (A) was moved to second row (B), and so on to dilute the sample. Nitrocellulose paper was soaked in buffer C before assembly. Samples were loaded into the apparatus and run through, 4X 150 µl of buffer C was added and left to run. Once all samples had run dry, Nitrocellulose paper/membrane paper was left overnight in buffer D. Buffer D was removed, the membrane washed twice with 1X PBS. The protocol then followed as seen in western blot section 2.4.2.

Chapter 3) Results of initial plasmid and protein testing.

3.1 Verification of plasmids

The plasmids used during this project were taken from previously made glycerol stocks. The plasmids were sent to Source Bioscience for sequencing to confirm the presence of the mutations and to check for deterioration. Figure 6 shows the primary sequence of the four different rhodopsin mutations. The full plasmid sequence was analysed and showed little to no deterioration or further mutations to the sequence. With this validation, we moved on to increasing the amount of DNA present to allow for the transfection protocols.

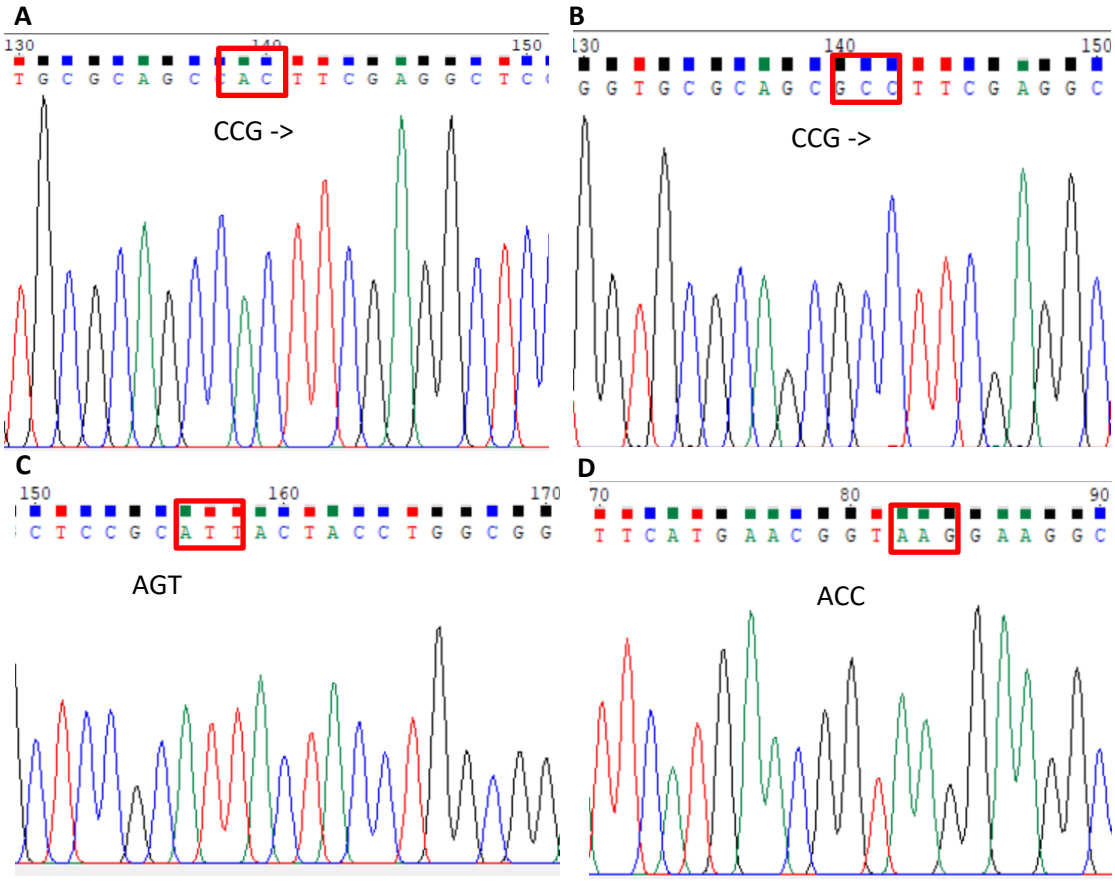

Figure 6 The sequenced plasmid DNA of mutated rhodopsin. This diagram was created using snap gene. The sequences are the forward strand in the 5'→ 3' direction, using primer F1 (SEQF1) A) P23H, B) P23A, C) Q28H D) T4K. The mutation can be seen highlighted in red with the original and new sequence in the black box below. These mutations are located on the N terminus of the rhodopsin protein.

3.2 The production and separation of the rhodopsin protein with subsequent calculation of yield.

DNA was amplified for the use of transient transfection to obtain rhodopsin samples. The calcium-phosphate method of transfection was chosen due to its reasonable efficiency and low cost. The cells were treated with -*cis*-retinal to rescue the mutated rhodopsin, as this has been proven to help the rhodopsin to fold sufficiently. In vivo the retinal is 11-*cis* but 9-*cis*-retinal was used as an alternative since the expense of using 11-*cis*-retinal is high and they have similar structure and interactions with rhodopsin (Sekharan, 2011). This causes no real difference to the results; however, the UV VIS Spectra will be slightly left shifted with full rhodopsin showing at 490nm, not 500nm as is shown for 11-*cis*-retinal.

Figure 7. shows the visible UV spectra of transiently transfected WT-rhodopsin. Figure 7.A is the original output showing both the dark spectra and bleached spectra together, this image was then magnified to produce figure 7. B with the intention of seeing a clearer difference between dark and bleached spectra at 490nm. The difference spectra can be seen in figure C.

Figure 7. A has a peak at 280 nm which is roughly 0.7, however we cannot see a clear peak between 490-500 nm which indicates low yield of rhodopsin. Figure 7.B shows a significant difference between the dark and bleached spectra indicating that some rhodopsin has been produced from the transfection, however a cleaner peak would be preferable. Figure (7.C) shows a clear peak between 490nm and 500nm, indicating a good yield of rhodopsin.

The concentration of the rhodopsin was calculated for figure 7.C as follows;

Using the absorbance of the peak at 490nm from the difference spectra and the beer lambert law, assuming total volume: 1,500 µl, molecular Wight of rhodopsin: 40,000, Extinction co-efficient of rhodopsin:40,600 and path length:1.

The sample used for figure (3.2.1) was a dilution: 150µl into a 500µl – a 10X dilution.

The highest difference was 489nm having an absorbance of 0.005151

$0.005151 / 40600 \times 1 = 1.268X10^{-7}$

$1.268X10^{-7} \times 40,000 \times 1,000 = 5.0748$ µg/ml

$(5.0748/2) \times 10 = 25$µg in 500µl

In the total sample of 1,150µl we would have 76.12 µg

This is a low yield, the expected would be to have ~60µg within a 500µl sample.

The 280nm peak visible in figure 7.A is caused by aromatic side chains, such as tryptophan and histidine, so is a good indication of protein presence. The protein measured in this peak can also be from contaminants and so can be used to monitor cell count at transfection level. In this instance from figure 7.A we see a peak of 0.7 given this sample is at a dilution of 10x, we can assume this is a very high cell count. The number of cells at the time of transfection is important and a high density of cells can lower the protein yield. This peak could indicate that a lower number of cells would be needed to increase efficacy. The transfection protocol was run multiple times and adjustments such as cell density were made throughout the project to obtain the highest possible efficiency and thus yield of rhodopsin.

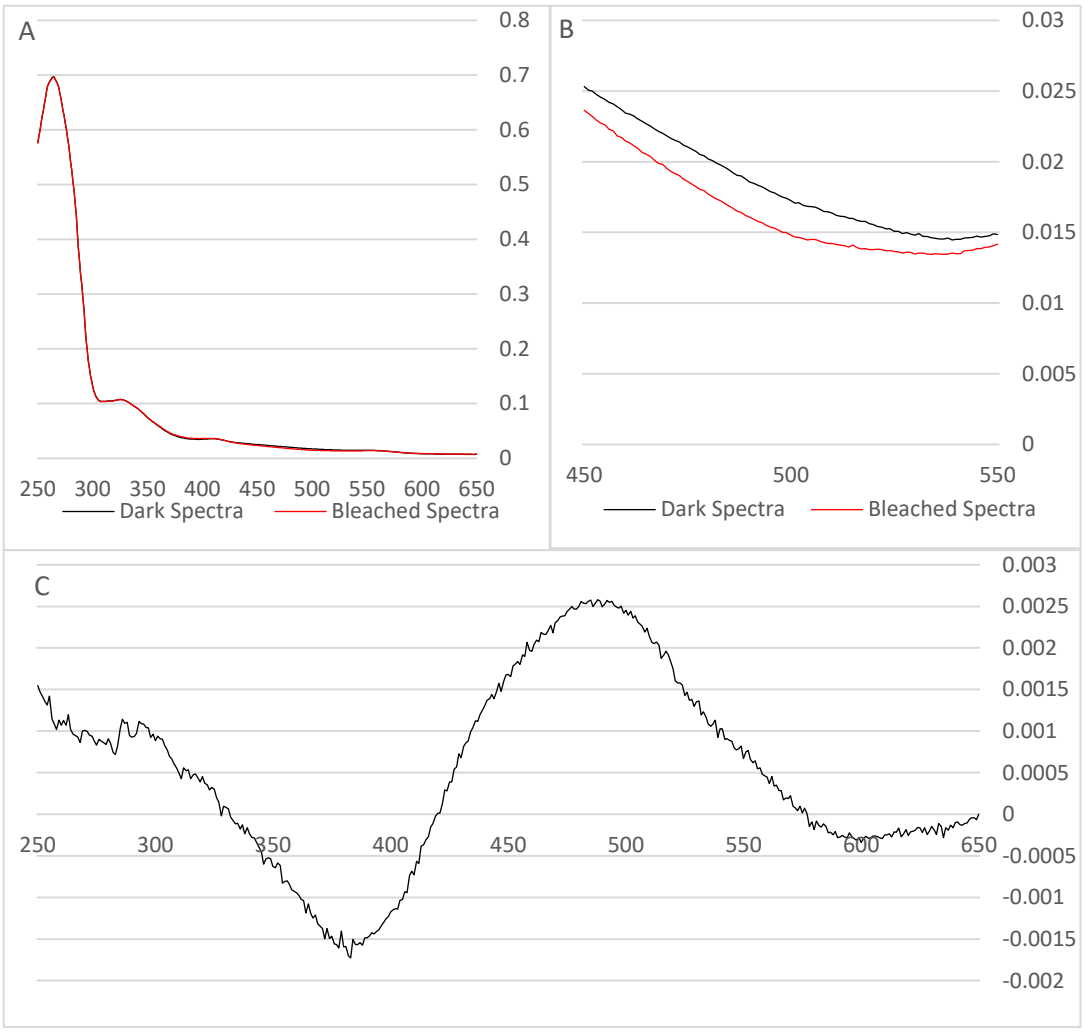

Figure 7 Wild-type control absorbance spectra. UV spectroscopy of harvested Hek293s cells which had been previously transfected with plasmids containing wt-rho. The cells were transfected using the calcium method, pre-prepared 9-*cis*-retinal was added to the rescued cells during the transfection protocol 48 hours before harvest, additional retinal had been added to all samples prior to testing as stated in methods. The samples were run before and after bleaching for 1 minute. For (A) and (B) Dark samples are black, bleached samples are red, the results had been zeroed prior to creation of the graphs. (A) The UV spectra output of Wt-rho, between 650-250nm, (B) zoomed in clearer graph of (A) showing wavelengths 550-450nm, (C)The difference spectra, calculated by taking the bleached spectra away from the dark spectra.

Figure 8 is the difference spectra of the harvested rhodopsin mutants obtained from transient transfection. Figure 8 1.A-D is to magnify the peaks at 490nm and Figure 8 2.A-D is to show the best comparison of the peaks at 490nm. We can see that P23A, figure 8. B had the highest concentration, 151 µg in 1.2ml. The second highest concentration was shown by Q28H at 71.3 µg followed by P23H at 20.7 µg and finally T4K with 16 µg in 1.2ml aliquots.

This agrees with the paper (Opefi, et al., 2013) which found P23A to be the most receptive to retinal rescue and managed to get the mutant to express at WT levels. Unfortunately, we can't definitively state that we managed to obtain WT levels of P23A due to inconsistency of the rhodopsin concentrations obtained from the transfections. The (Opefi, et al., 2013) paper also managed to express T4K at the same levels as WT we did not find this to be the case, this could be due to poor transfection or low quality DNA which as previously mentioned have an effect on the concentration of rhodopsin harvested.

The 280nm/490nm ratio also known as the purity ratio as previously mentioned can be used to assess the efficiency of transfection, but it can also be used to monitor the degree of misfolding. The ADRP mutations chosen misfold within the ER leading to little production of rhodopsin, the 9-*cis*-retinal rescue aids in the folding of the protein leading to a lowered degree of misfolding and an increase of rhodopsin production. The increase of rhodopsin concentration and the increase of purity ratios are signs that the transfection and thus the retinal rescue worked well. The retinal rescue working means that the degree of misfolding has been lowered for the protein. We can compare these results of the mutants to each other to determine which of the mutants have the highest degree of misfolding. It is important to look at all results before determining this as many variables can effect the results obtained from the transfection.

From figure 8 using the dark spectra of these samples we found ratios of 0.07 for Q28H, 0.05 for P23A, 0.05 for T4K and 0.004 for P23H. The high purity ratio for Q28H would indicate that this has the highest efficiency and thus the lowest degree of misfolding. From other papers we know that this has not been found to be the case, thus we must look at the wider picture. The absorbance at 280nm for each of the mutants were as follows: 1.14 Q28H, 1.505 P23A, 1.18 T4K and finally 0.68 P23H.

Taking these into consideration we can see that P23A and T4K had the same ratio, which would indicate the same efficiency of transfection despite having large differences in concentration. Looking at the 280nm absorbance for P23A and T4k which was 1.505 and 1.18 respectively we can see a large difference, the peak at 280nm is caused by aromatic side chains and so show the presence of protein, this can include contaminates. The difference in size of this peak can mean that there were not enough cells present at the time of transfection of T4K and thus the yield of rhodopsin is lower. This difference can also be slightly attributed to the increase of rhodopsin within the P23A sample. There is however clearly a discrepancy in the transfection of T4K, the cell density will have to be improved, in-order to increase the yield of rhodopsin and thus be in agreement with the (Opefi, et al., 2013) paper. P23H had the lowest absorbance and purity ratio and a low concentration of rhodopsin. There is clearly a fault with the transfection of this mutant, the cell density at transfection was obviously far too low and needs to be increased. Q28H produces the biggest outlier having been shown to only reach levels of ~50% of WT-rhodopsin (Opefi, et al., 2013), yet showing higher concentrations of rhodopsin than that of T4K it is most likely that the transfection for this mutant went far better than that of the others and thus gives the impression of a lower level of misfolding. If the objective had been to ascertain the level of misfolding further experiments of biochemical characterisation would have shown better the degree of misfolding despite the apparent high concentrations noted here.

Figure 8.D does not follow the standard shape, the rhodopsin peak at 490nm is low and broad and the graph does not dip at 390nm as is seen in figure 8.A-C. This could indicate low yield, an excess of contaminants due to high cell count, or problems with the UV Vis Spectroscopy machine, which had a habit of overheating. The sample aliquot also had a high dilution of 12x which may have influenced the ability of the old machine to detect the low amounts of rhodopsin present. This may have affected the concentration calculated for T4K.

It is important to note the difficulties that occurred while trying to increase the yield of transfection including cell count, buffer failure, and low-quality DNA.

Transfections were tested to find yield and roughly determine the cell count. The values at 280nm together with the protein concentration calculated from the peak at 490nm, are good indicators for cell count. It is possible to tell how well the cells were transfected, as a high peak at 280nm and a low protein concentration (peak at 490nm) can indicate that there were too many cells at the point of transfection. Low yield can also indicate that there were problems with the transfection itself such as; poor quality DNA or poor buffers. For the protocol used however it is most commonly the cell count that leads to poor 280nm and 490nm ratio, with a much lower 280nm indicating not enough cells. The expected value for 280nm in the case of 10cm plate in this instance is about 0.6 with the larger plates 15cm not bigger than 1/1.2. From this information we were able to work out the efficiency of the transfection and possible changes that needed to be made. The problems started when we began scaling up to using larger plates. In the end the cell count was determined to be the reason behind the low yields, having either too many or too few. We had to rule out however the likelihood of another factor, so new midi prep kits were used to increase the yield of DNA and its quality and new buffers were brought up. Finally, it is key to note that the protein yield for these mutations is characteristically low regardless.

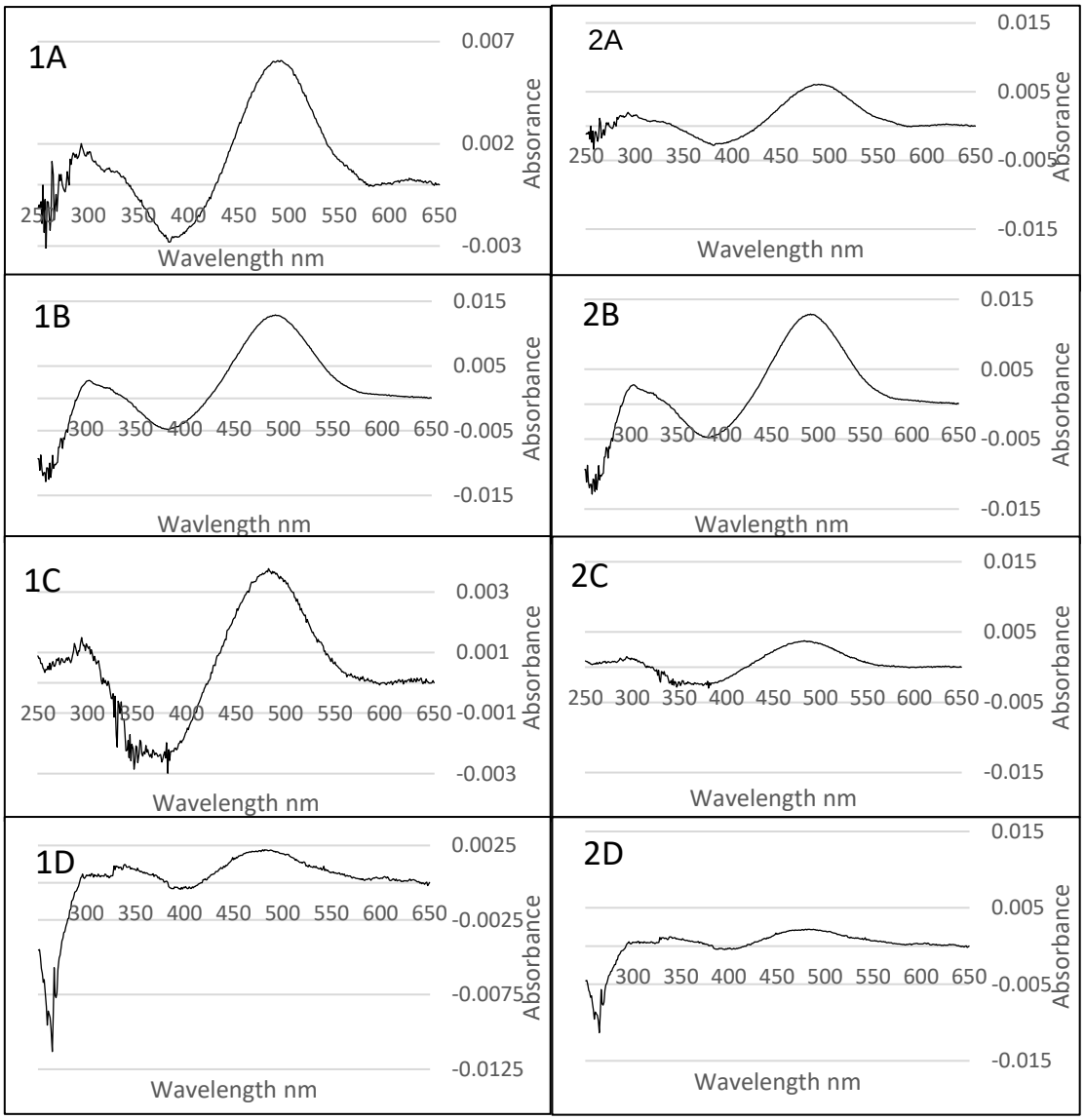

Figure 8 The difference spectra of transient mutant rhodopsin Q28H (A), P23A (B), P23H (C) and T4K (D). Figures 1A-D are shown to magnify the peak and figure 2A-D are to compare the peak size, the same samples are used for both. These mutants were transiently transfected into HEK293s cells using the calcium method and were rescued using 9-*cis*-retinal. The mutants were harvested and frozen and their spectra checked. The difference spectra was found by measuring the sample before and after photobleaching to locate the amount of rhodopsin present. A 12x diluted aliquot of the sample was used (100µl of 1,200 µl). The concentration of rhodopsin was calculated and is as follows; Q28H (A) 71.3 µg, P23A (B) 151 µg, P23H (C) 20.7 µg and T4K (D) 16 µg in 1.2 ml.

3.3 Ascertaining the presence of rhodopsin and its cleaved portions within samples

The samples were analysed by western blot to show the presence of both full rhodopsin 40kDa and the truncated species, which as previously mentioned was found to be at roughly 27kDa (Tam & Moritz, 2007) making the corresponding species 13kDa, however this species has not been identified on western blot analysis before.

As can be seen from figure 9 there is rhodopsin present in P23A, P23H, WT-Rho and T4K samples. Figure 9.A shows a strong band at 40kDa (rhodopsin) for P23A non-rescued. The bands for P23A on figure 9.A seem to follow the same pattern, however the intensity of the bands for non-rescued seem to be higher than those of the rescued sample, it is likely that due to human error these samples were accidently switched. Figure 9.B shows a lower intensity for non-rescued P23A which would again support the theory that the rescued and non-rescued samples for P23A in figure 9.A may have been swapped. There is not a band at 28kDa for P23A in either figure 9.A or B however there does appear to be a band below 40kDa for none rescued and rescued P23A in figure 9.A it is possible that these bands are the truncated form and that if the sample had been left to run longer we may have seen the band at 27kDa. There are bands below that of 35kDa for the rescued P23A sample in figure 9.B and a weaker one at the same distance for non-rescued P23A, it is possible that the band in the non-rescued sample is simply a shadow band but given such similarities in distance it is possibly the truncated rhodopsin.

There is a clear difference in the bands seen for rescued and non-rescued P23H in figure 9.A and 9.B, this is to be expected. In figure 9.A we see rhodopsin present for both rescued and non-rescued and the appearance of a possible lower band for the rescued version, again we can't be sure as the sample was not left to run long enough. In figure 9.B we only see clear bands for rhodopsin in one of the rescued versions, this sample however appears to have a clearly distinct band lower than that of the expected

40kDa for rhodopsin, this band cannot be considered a shadow band and so is very likely to be the truncated version. This supports the theory that the western blots do show the truncated species but were not run long enough to show a definitive weight.

There were no bands produced by non-rescued T4K in figure 9.A there is however a slight band shown for the rescued sample. This weak band is likely due to low concentration of the sample used. Figure 9.B shows clear and distinctive bands for T4K clearly showing the presence of rhodopsin in both rescued and non-rescued forms. It is interesting to note the intensity of the final band for rescued T4K at around 35kDa, this band is expressed weakly in the non-rescued version and is possibly the truncated form of rhodopsin.

We can clearly see the three bands for the trimer dimer and monomer of rhodopsin for WT in both figure 9.A and B. There is no noticeable difference between the intensities of rescued and non-rescued WT in either figure 9A or B, this highlights the difference noted between the rescued and non-rescued versions of the mutant rhodopsin. Using WT as a comparison we can see that there are no bands lower than 40kda in any of the WT samples for figure 9.A, with only one band lower on figure 9.B non-rescued WT which is most likely a shadow band due to the fact there is no replication of this band on any of the other WT samples, again highlighting this difference in the mutant forms and thus providing more evidence that these lower bands are likely to be the truncated form of rhodopsin.

If we compare the samples in figure 9.B we can see that the lower bands on T4K non-rescued and rescued, P23A rescued and P23H rescued are all at the same hight lower than that of the shadow band located on WT non rescued sample. I believe this is proof that the truncated form is present in each of the mutated samples to some degree.

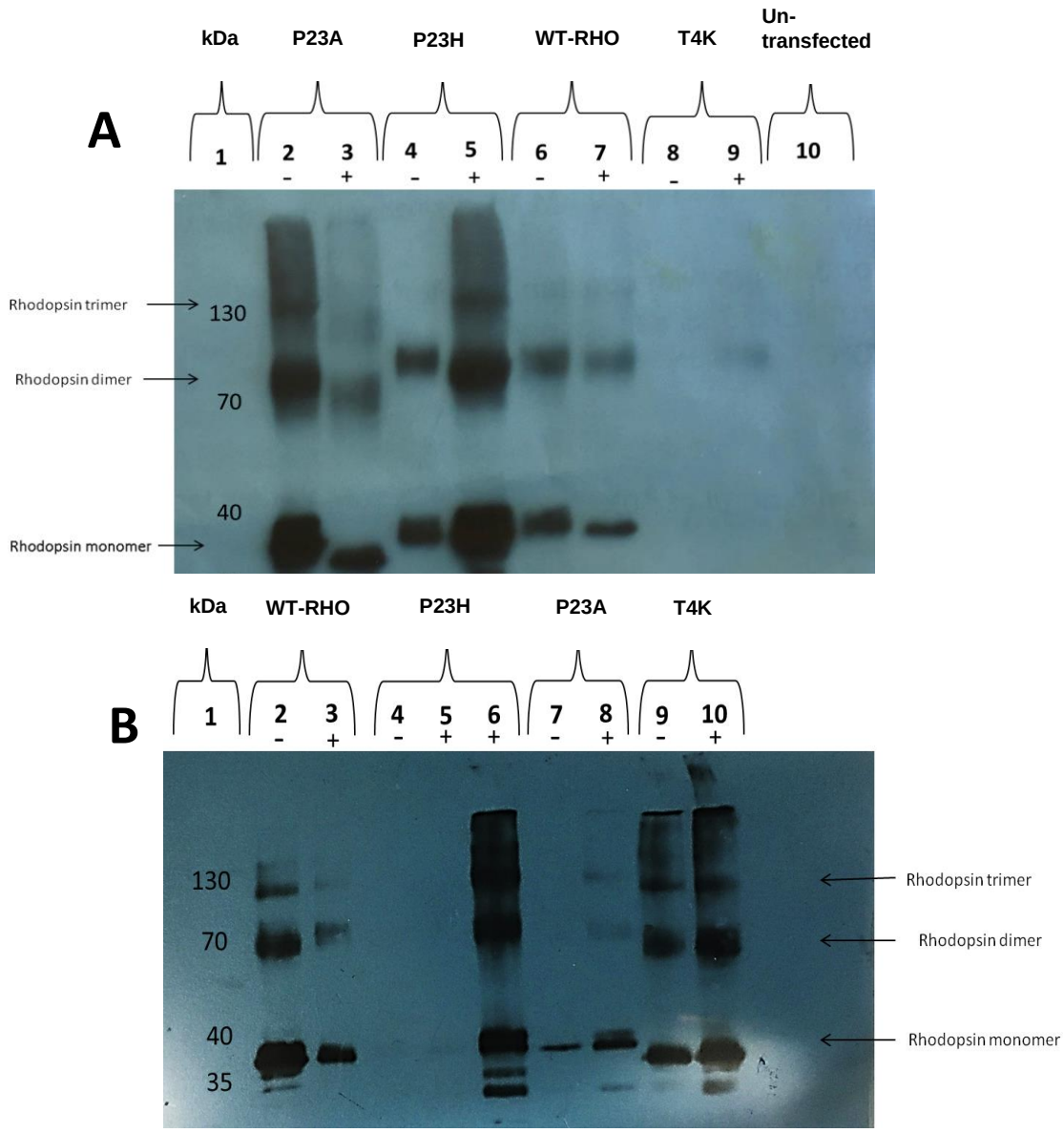

Figure 9 Western blots of WT and mutated rhodopsin samples harvested from transient transfection. The labels above each of the lanes indicates the type of mutation and the + and – is used to indicate if the sample was rescued. Those that have been rescued were treated with 9-*cis*-retinal l during transfection. These samples have been transfected using the calcium chloride protocol and were harvested in PBS. They were all treated with further retinal after harvest before testing via UV VIS Spectroscopy and then analysed further by western blots, using 1D4 as the primary antibody.

3.4 Attempted creation of A stable cell line for mutants P23A and P23H using Hek293s cells.

A stable cell line was attempted to increase the efficacy of the project. The long transient transfection protocol meant that many hours were spent trying to produce the mutant protein. The separation protocols required a high concentration of protein to work well. The mutants P23A and P23H were chosen to create a stable cell line.

A stable cell line for WT rhodopsin has been made before using the following papers (Reeves, et al., 2002) (Reeves, et al., 2002). Following much the same procedure, it was attempted to make P23H and P23A stable cell lines.

Following the methods section 2.2.8, we managed to transfect the cells so that they were able to produce the desired P23H/A mutant rhodopsin, had geneticin and blasticidin resistance and were inducible by tetracycline. This was made possible using the plasmid pACMV-*tetO*-P23H/A, which was produced following the methods used in (Reeves, et al., 2002). The HEk293 cells were transfected with the Tet operon repressor protein and blasticidin resistance. Those able to take up this plasmid were resistant to blasticidin which was the first marker used, followed by geneticine testing and finally the cells were induced using tetracycline. It is possible that at any of these stages of selection, the process had not been fully successful as any cells allowed to multiply without the resistance for these antibiotics couldn't go on to form the stable cell line or produced the desired protein.

Figure 10, shows the dot blots that were created using samples from the stable cell line experiment. Figure 10.A shows the outcomes from the P23H experiment, and figure 10.B shows those of the P23A experiment, each pair of dots represents a different colony collected, for each mutant we tested 11 samples. The positive and negative symbols represent those induced by tetracyclin and those not induced respectively. Thus we should get higher intensity dots for the positive columns. The samples are diluted as we move down the coloumn, this means that the dot blots

should show a gradual decrease in intensity as the protein becomes more and more diluted. We also have a positive and negative control depictied with PC and NC respectively. The PC is the rescued T4K sample used for figure 9.B and the NC is a sample of harvested un-transfected cells.

Figure 10.A shows no positive result with the negative control expressing with the same intensity of the other samples. We can clearly see an increase in intensity of the dots shown for the positive control which have not been duplicated in any of the other samples. Leading to the conclusion that none of the P23H samples contained protein and so we failed to produce a stable cell line for P23H.

Figure 10.B has one high intensity dot, on the last row of the second column, given that it is the final dot of this column and that the intensity should decrease as we move down the dots it is interesting that this seems to have so much protein present. When we compare this dot to the positive and negative controls we can see that the intensity of the dot in the second column mimics that of the positive control. The other dots in figure 10.B match that of the negative control, showing that no protein was detected in the other samples. This dot blot would need to be repeated to be certain of the presence of protein.

It is important to note that there is a possibility that the experiment was successful but due to poor induction of the cells it cannot be seen clearly on the dot blot. This could have been tested by bringing up the cells again until confluent and inducing them, running another western blot analysis, and seeing if this made a difference. There was however time sensitivity issue with this project and it was thought best to not continue testing as we had to complete the two rounds of immunoaffinity chromatography.

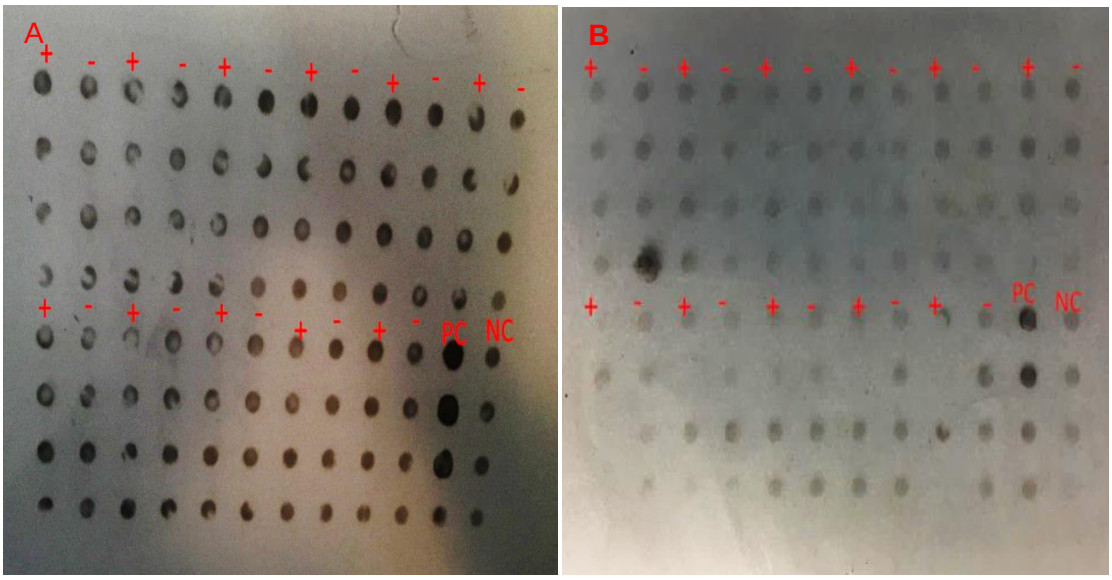

Figure 10 A dot blot of colonies collected from stable cell line transfection of P23H and P23A. This dot blot contains samples from different colonies of the attempted stable cell line P23H (A) and P23A (B) mutant type rhodopsin, both with induction (+) and without induction (-) to show the expression of the mutant rhodopsin. These cells were brought up with blasticidin resistance, the cells were then transiently transfected using the described Teto- mutant type plasmids. The cells were then tested for Geneticin resistance and left to form colonies. These colonies were then isolated before being re-plated into 24 well plates, split thrice upon confluence, for freeze down, induction and non-induction. The induced and non-induced samples were transferred to mirocentrifuge tubes and spun for storage at -20. On the far right are the positive and negative controls which were previously made up from transfection protocols, the PC (positive control) is the T4K mutant which had on a pervious western blot shown good expression, the NC (negative control) is of an un-transfected cell which also underwent the same procedure as the positive control without the addition of DNA. The Dot blot was carried out as described fully in the methods section.

Chapter 4) Results of purification of truncated rhodopsin

The main objective of this study was to isolate and analyse the truncated forms of mutated rhodopsin. As previously established in multiple studies and explained in the literature review, rhodopsin with mutations in the N-terminus can be pharmaceutically rescued using the chromophore, vitamin A derivative; 11-*cis*-retinal. This rescue however is believed to lead to the protein being cleaved by proteasomes at the N terminus. To prove this, two different forms of immunoaffinity chromatography were utilised, this was done with the hope of separating out the desired truncated rhodopsin. As discussed, it is our belief and that of others that the P23H mutant truncates in-order to stabilise the rhodopsin protein so that it can be trafficked through-out the cell (Tam & Moritz, 2007). The mutants chosen are all located within the N-terminus to try to show that all mutants located in the N-terminus followed this pathology.

Chromatography is a method of separating out a desired protein. The initial step is to set up a method by which the protein can be identified and isolated, there are multiple forms of chromatography which utilise different properties of the protein for instance Ph level, charges and size; in the case of affinity chromatography the aim is to bind to a specific ligand. Affinity chromatography is a well-established method which exploits biological-like interactions of the desired protein to isolate it out of a liquid. After finding a suitable ligand it is chemically immobilized onto a stable support, this will allow the protein when bound to stay within the affinity column rather than to wash through still bound. The ligand now bound to the support is normally suspended in a liquid and this solution is known as a slurry. The protein mixture is made up with the specific conditions so as to increase binding affinity to the ligand. The slurry is then added to the mixture of proteins and is incubated often at specific temperatures and on a rotator to mix end over end to increase binding. Once the mixture has been left for the appropriate amount of time the mix is poured into the affinity column and the liquid is allowed to be run through. The proteins are then washed a number of times

dependent on the size of proteins or the size of the column to ensure only the bound protein is remaining. An elution buffer is made up which usually contains a different set of conditions which will loosen or dissociate the desired protein from the ligand, or in some cases contain a competing protein which will bind instead to the ligand. The result is the purified protein is eluted off with minimal to no contaminates. This is clearly represented in figure 11, which shows the general system used for separating out proteins using affinity chromatography (Scientific, N.D).

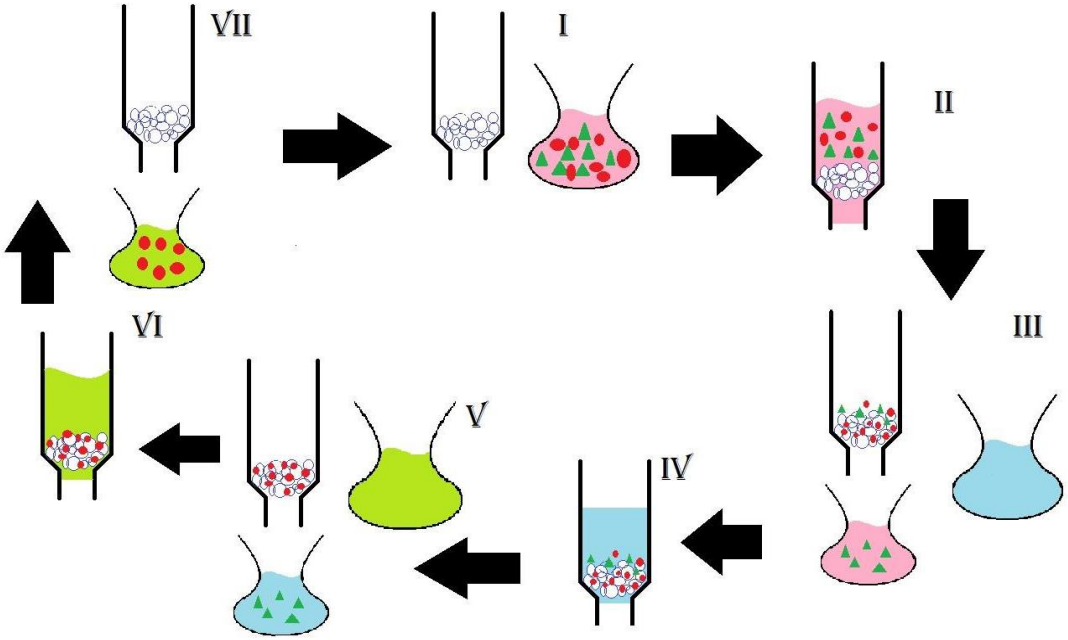

Figure 11) The basic structure of affinity chromatography. I) Shows the column, and the mixture of proteins. II) shows the solution being added to the beads and being allowed to flow through the column at this point the undesired proteins are beginning to flow through. IV) the wash is added to the column to remove the rest of the unwanted contaminates. V) The wash is allowed to flow through removing the remaining unwanted proteins, leaving only the bound desired proteins. VI) The elutant is added and it competes with the proteins to bind the lectins which are attached to the beads. VII) The elutant is then run through allowing for the separation of the desired protein.

In this case the protein we wish to separate is rhodopsin. It is hypothesised that 11-*cis*-retinal in the ER allows for the pharmaceutical rescue of the mutated rhodopsin allowing the protein to fold and leave the ER. It has been shown that ADRP rhodopsin cleaves at the N-terminal cap to increase stability, the identification of truncated P23H rhodopsin has already occurred, however as of yet we know little of the fractions of rhodopsin how they occur and what protein kinase cleaves them (Tam & Moritz, 2007). To answer these questions, I wanted to isolate the different variations of this cleaved form of rhodopsin, assuming at the time that the truncated mutated rhodopsin will have lost its glycosylation sites. I have utilised two forms of Immunoaffinity chromatography, one which binds to the TETSQVAPA sequence located on the C-terminus of rhodopsin (1D4-Rho) and the second Con-A which binds to mannose sequences on the N terminal Cap. The immunoaffinity chromatography separations were run consequtively. The first separation purifys the sample, 1D4 as mentioned attaches to the carboxylic end of the protein. This means that in the elutions form this separation should comprise of all rhodopsin with a c terminus, leaving us with the truncated form and the full rhodopsin. The second separation will only bind to those with an N terminus, given that we believe this has been cleaved off the truncated form, the elution for this column should only contain full rhodopsin. The wash through and initial run through of the sample should then contain all the truncated rhodopsin. The basic flow through of how we intend to separate out the truncated mutant can be seen in figure 12.

These were both originally tested using purified ROS Rhodopsin, thus we could asses if the buffers or apparatus used caused degrading of the protein. It was however assumed that regardless of the success of these preliminary tests that the recombinant WT and the recombinant mutants would be harder to isolate.

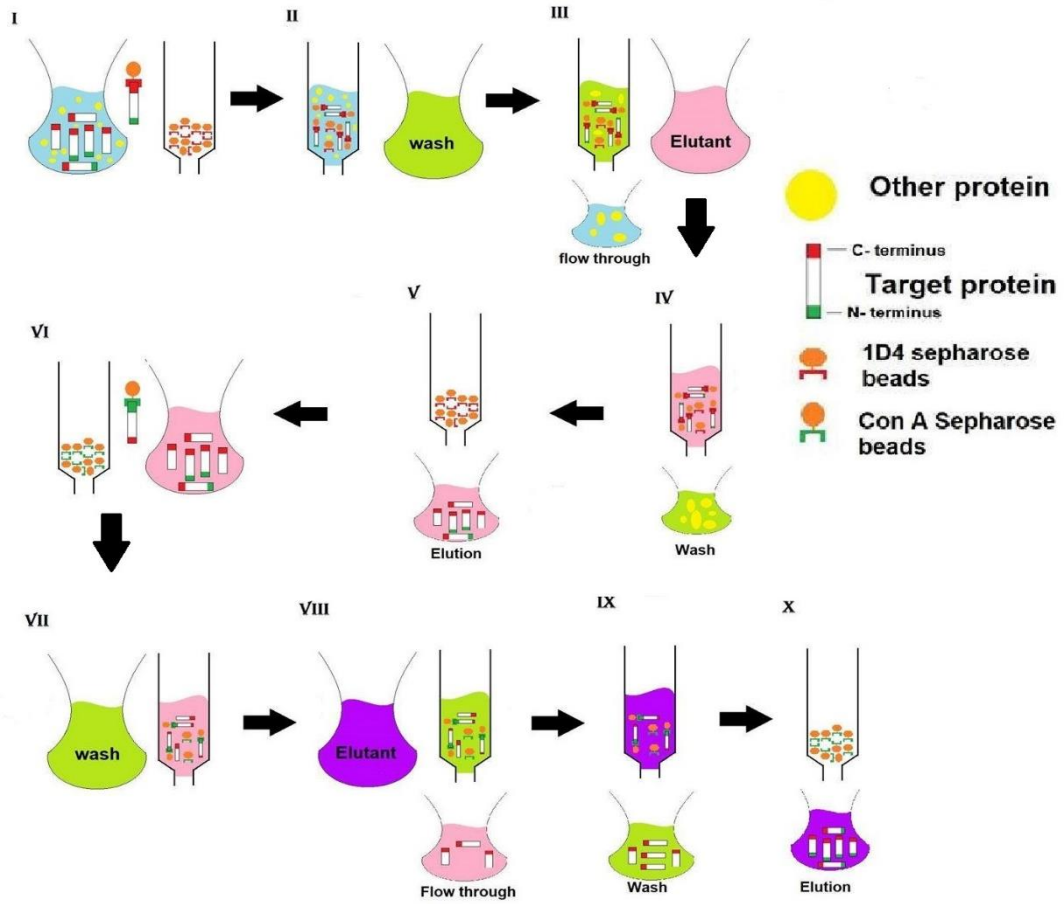

Figure 12 The basic flow diagram of the method used to isolate out the truncated mutant rhodopsin. I) The mixture of proteins with the C terminal in red and the N terminal in green, the 1D4 beads within the column and an image of the rhodopsin attached to the 1D4 beads on the C terminus. II) The rhodopsin now bound and the prepared wash. III) The flow through with the wash now added to the column and the elutant prepared. IV) The collected wash and the contaminants that came with it. V) The elution containing all separated rhodopsin. VI) The Con A beads prepared in the column and an image of the Con A sepharose beads bound to the N terminal end of the rhodopsin. VII) The 1D4 elution added to the column and the prepared wash. VIII) The flow through including some of the truncated rhodopsin mutants with no N terminus, the wash added to the column and the prepared elutant. IX) Shows the collected wash with more of the unbound truncated mutant rhodopsin and the elutant added to the column. X) The elutant containing all the full rhodopsin species, with the con A beads in the column

4.1 1D4 separation protocol

The 1D4-sepharose bead separation protocol has been widely analysed and thus the protocol for this has been well established, and was described previously in the methods. A preliminary result was taken using purified ROS rhodopsin to verify the efficiency of the protocol.

Purified ROS rhodopsin was used to run the first purification protocol as a control to ensure highest efficiency possible and to make any changes to the protocol prior to using the cell extract samples gained. Prior to purification, UV Vis spectroscopy was run on the ROS rhodopsin to identify the concentration of the sample. This protocol was followed slightly differently from the other UV Vis spectroscopy as the sample used did not need to be lysed, thus 20 µl of the sample was diluted by PBS into a 500µl sample for UV spectroscopy. This ROS rhodopsin was formed with 11--*cis*-retinal rather than 9-*cis*-retinal so the peak is identified at 500nm, not at 490nm. The UV Spectra from this experiment can be seen in figure 14A-C, which clearly show the rhodopsin peak.

In Figure 14 A and B we can clearly see the difference between the dark and bleached spectra, with a much neater shift of the 500nm peak than in the transient transfection UV Spectra seen for WT in figure 7.A. The calculations for the spectra were conducted as previously explained and the purification protocol was then run. The output for the purification protocol can be seen below in figure 14.D, the protocol was run using 100 µg of the sample.

Figure 14.D shows the elutions taken from the purification protocol, to see the purity of this sample the 280/500nm ratio was calculated. The absorbance at 280nm was 0.206392 and the absorbance at 500nm was 0.115069, thus the ration of purity was: 0.55. An ideal purity ratio is around 0.6.

The concentration of rhodopsin from the UV Vis spectra was calculated as follows.

For the calculations assume that the total amount in the sample is 100 µl. 20 µl is added to the 500µl sample a 5X dilution.

The highest value is at 501nm absorbance 0.073887

$0.073887/40600 \times 1 = 1.819 \times 10^{-6}$

$1.819 \times 10^{-6} \times 40{,}000 \times 1{,}000 = 72.795$µg/ml

72.795µg/ml 2 = 36.39µg per 500µl

36.39 x 5 = 181.9876µg in the final sample.

An aliquot of roughly 150 µg of this was then taken to perform the separation protocol as seen in figure (14.D). The concentration of the elution was then calculated

Elution 1 absorbance at 500nm – 0.115069 leads to 113.3 µg in 500 µl

Elution 2 absorbance at 500nm – 0.031807 leads to 31.3 µg in 500 µl

Elution 3 absorbance at 500nm – 0.008544 leads to 8.4 µg in 500 µl

Elution 4 absorbance at 500nm – 0.005 leads to 5 µg in 500 µl

The total rhodopsin eluted was 158 µg, this would indicate that there was a problem with calculations which could have been avoided by double checking concentration prior to elution. It is also possible that the calculations aren't exact as checking concentration in this manner is not specific, if this is to be believed then protocol efficacy is near 100%.

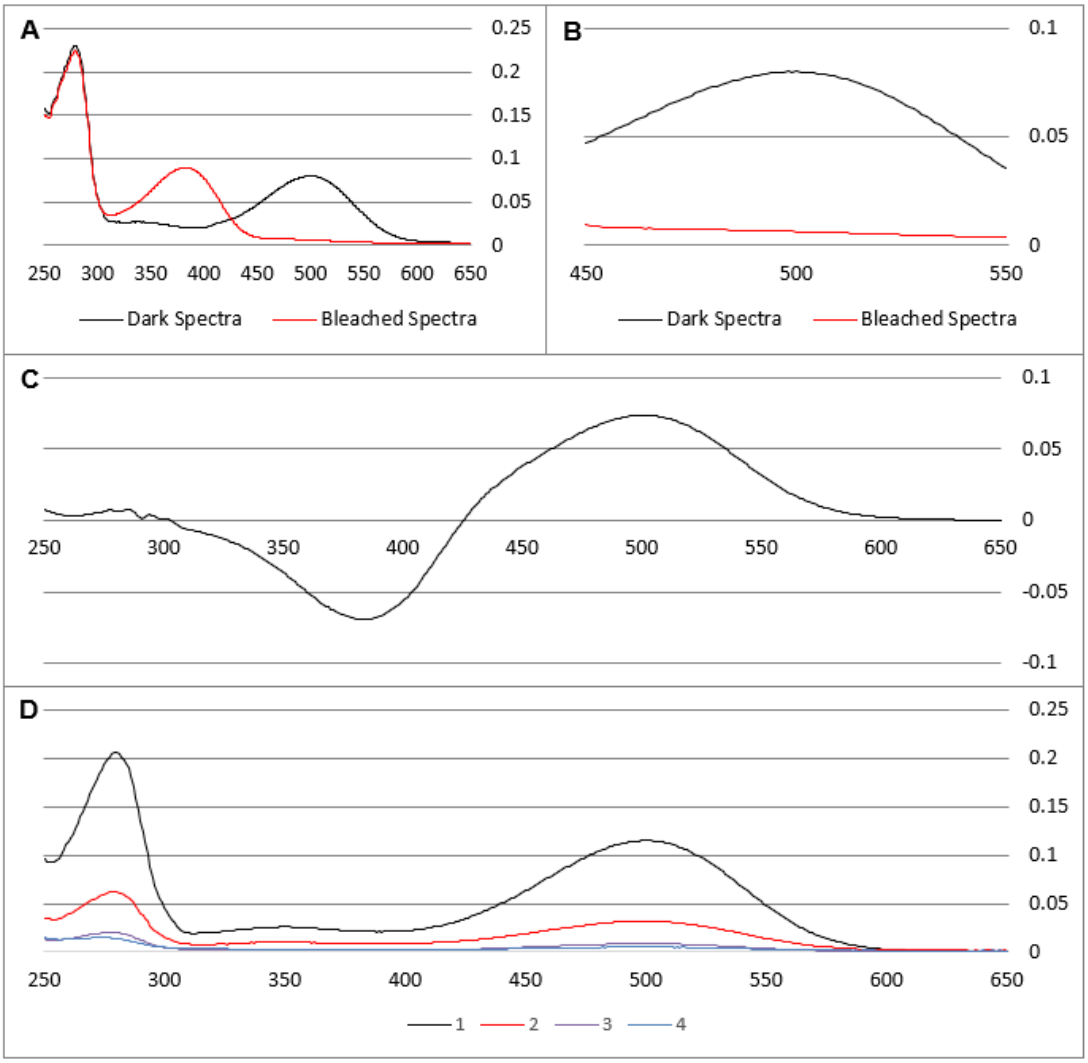

Figure 13 (A-C) WT ROS rhodopsin control absorbance spectra and (D) absorbance spectra of the 1D4 sepharose separation elutions from this sample. The UV vis spectra obtained using purified ROS rhodopsin. A) ROS rhodopsin was diluted using PBS: 20 µl into 500 µl to obtain the dark and photobleached UV vis spectra, the rhodopsin present can be clearly seen by the peak at 500nm and the metarhodopsin II state can be seen at 380nm. B) A close up of the graph seen in A to show the difference between dark and photobleached state. C) the difference spectra obtained from figure 14 A by taking the bleached spectra away from the dark spectra to calculate the exact amount of rhodopsin present: 72.795 µg. D) Once the concentration of rhodopsin was ascertained a small aliquot of this was then used for 1D4 –sepharose separation, the elutions are taken in order 1, 2,3 and 4.

Figure 14 A-D are the elution fractions of the 1D4-sepharose separation protocol of the mutant rhodopsin. Figure 15 A-D are the results from the elution fractions of figure 14 A-D, showing fractions against absorbance at 490nm, presenting clearly the flow of rhodopsin through the separation protocol.

Figure 14.A (Q28H) shows a clear peak on elution 1 and shows much smaller broader peaks for elution 2 and 3. This can also be seen in figure 15. A which shows a high peak at the first fraction (elution 1) and then shows a small secondary peak at fraction 4 (elution 3). There is a consistent level of rhodopsin showing throughout the separation, with the wash fraction showing higher levels of rhodopsin than the fractions of elution 3 and 4. This could mean that not all rhodopsin was bound due to 1D4-sepharose beads leading to washing out of the rhodopsin. The consistent high absorbance could also be due to inaccurate blanking or overheating of the UV/VIS chromatography spectrometer. The purity ratio was calculated at: 0.36 and the concentration of rhodopsin was 16.2μg.

Figure 14 B (P23A) again shows a clear peak for the first elution with a secondary smaller peak for elution 2. The purity ratio was calculated at 0.26, this is significantly lower than desired. Figure 15. B emphases the peak at elution 1 but does not highlight the peak that can be seen at elution 2. The wash fraction is below zero which again could be indicative of blanking error or machine failure. The wash fraction has lower absorbance than that of fractions 4 and 5 indicating low if not no concentration of rhodopsin present in the wash. This means that complete binding of rhodopsin occurred. There is also very little rhodopsin recorded in the elution 2 with no rhodopsin present in either elution 3 or 4, meaning that over 80% of rhodopsin eluted was eluted in the first elution.

Figure 14.C (T4K) shows a clear peak at 490 nm and a smaller and much broader peak present in elution 2. The concentration of rhodopsin in the first elution was calculated at 7μg with a purity ratio of 0.24. Figure 15 C allows for a clearer image of

this broader peak at elution 2, while highlighting the peak at elution 1. Interestingly we can see an increase of rhodopsin present in the fourth elution which when looking at figure 14.C is only slightly present but not shown as a peak. This result may have been due to elution buffer not being fully run through and left in the separation column increasing the concentration of the final elution. It may also simply be a machine error due to overheating.

Finally figure 14.D (P23H) shows a broader peak at 490nm and what appears to be a steaper increase to 280nm, this is not noticed in the other ADRP rhodopsin samples. This increase may be due to failure of the 1D4 sepharose coloumn to separate the rhodopsin from its contaminates. It is possible that for this sample more washes needed to be completed due to excess retinal. As the concentration of retinal added to the samples at transfection remains the same, if the concentration of rhodopsin harvested is lower the ratio of retinal to rhodopsin will change, and thus more washes will be needed to remove this excess. This could also explain why the purity ratio of elution 1 is 0.17, much lower than the other mutants tested. The other elution fractions however do not show this increase in 280nm, so it is possible that this result is simply an outlier. Figure 15.D highlights the wash sample, which is below 0, this again may be due to machine error or blanking issues, if we were to 0 this result we would see an increase in rhodopsin present throughout the rest of the fractions. We again notice the slight increase of rhodopsin showing in the final fraction.

Having a higher purity ratio for Q28H again is unexpected as previously explained in section 3.2, Q28H should show a lower purity ratio than P23A. It is likely that the quality of the DNA used for transfection of Q28H was simply higher than that used for P23A. This would explain the difference of Q28H to P23A while also explaining why T4K and P23A consistently have similar purity ratios as found in previous works.

Overall we can see from figure 15 that P23A had the best flow of rhodopsin, despite having a slightly lower purity ratio and concentration than that of Q28H. There appeared to be a constant flow of rhodopsin from Q28H which would indicate poor binding or a poor 1D4 slurry to rhodopsin ratio. It is interesting to note that the 1D4 separation appeared to work best for those more stable mutants P23A and T4K, with Q28H being an outlier.

We could improve on the elution process of the 1D4 separation by increasing the percentage of rhodopsin obtained in the 1st elution. The best way to do this would be to increase the amount of competing ligand in the elution or leaving the competing ligand longer to bind. The higher concentration obtained here will allow for a higher concentration to be used in rho-con A-sepharose separation and thus leading to a high concentration of truncated rhodopsin obtained. We must also increase the purity ratios; samples may have been affected by an increase of retinal contaminates. There was a high amount of retinal present in the mutant samples due to retinal being added before and after transfection. This meant that there needed to be an increase in the amount of washes compared to that of the purified ROS rhodopsin that was used to test the protocol. It is possible that more washes were needed and excess retinal remained as a contaminant which would of lead to an increase of absorbance at 280nm and thus poor purification ratios.

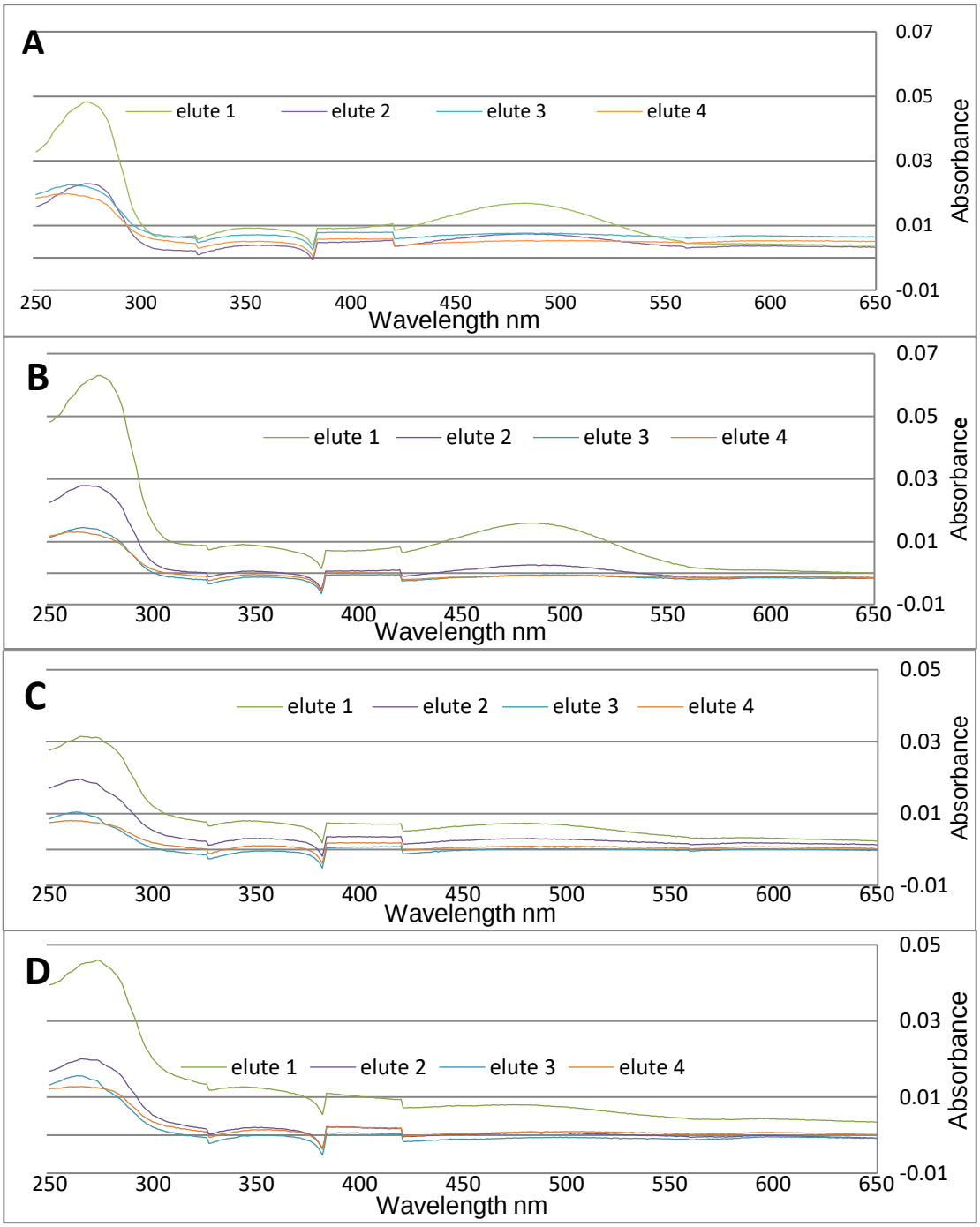

Figure 14 The elution of 1D4-sepharose separation protocol for the recombinant mutant rhodopsin. The rhodopsin was obtained via transient transfection and the initial concentrations were found using UV vis spectroscopy. The rhodopsin was then prepared for 1D4 separation as seen in the methods section 2.3.1, once bound they were washed of excess retinal and then eluted off. A, B, C and D show Q28H, P23A, T4K and P23H respectively. The absorbance at 490nm shows the rhodopsin present.

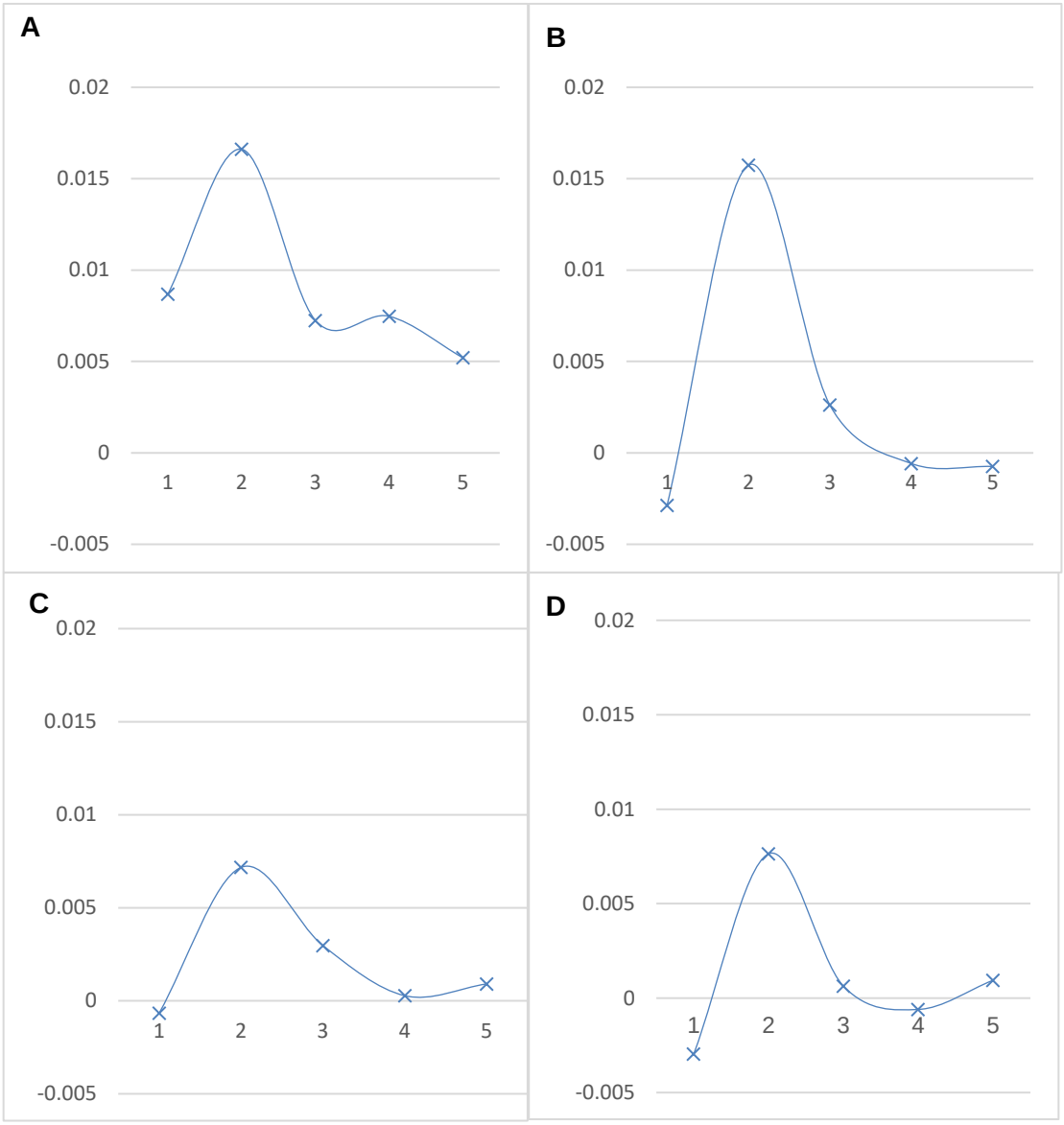

Figure 15 A chromatogram of rho-1D4-separation column of ADRP rhodopsin mutants. The rho-1D4-sepharose separation was conducted on previously harvested ADRP rhodopsin mutants, the rhodopsin was then bound to the 1D4-sepharose beads before being washed and finally eluted using competing ligand rho-1D4 peptide. The chromatogram shows the absorbance at 490nm for a wash sample and each of the elution fractions obtained from 1D4-sepharose separation, showing the flow of rhodopsin over the course of the separation. The full UV/VIS spectra of these elution fractions can be seen in figure 14. The fractions are 1-Wash, 2- elution 1, 3- elution 2, 4 -elution 3 and 5 – elution 4. The mutants are P23A, P23H, T4K and Q28H showing as A,B,C and D respectively.

4.2 Con-A separation protocol

Concanavalin A or Con A works by binding onto the Glycan moieties left behind by glycosylation. It was found that non reducing α-glucopyranosyl, α-mannopyranosyl or α-fructofuranosyl residues can be precipitated by concanavalin A (Ogata, et al., 1975). The oligosaccharide chains on rhodopsin are predominantly GlcNAc3Man3 with some containing Man4 and Man5 and have been shown in WT to bind to Con A as a method of separation (Shichi, et al., 1980). It is important to note that the four mutations that were used during this experiment; Q28H, T4K and P23A/H have all been proven to have effects on the glycosylation of rhodopsin (Behnen, et al., 2018) (Chen, 2014) (Sakami, 2011). This could cause problems as in order to separate out the truncated species of the mutated rhodopsin, the N terminus with completed glycosylation and thus glycan moieties intact must bind to the con A, if there are problems with this binding it could lead to contamination of the elution.

The Con A protocol was taken from multiple difference papers and then altered to increase efficiency. Originally focus was on the increasing % of binding of rhodopsin. This included analysing the time needed and the suitable amount of ions needed to create an environment that the protein could bind to the beads most efficiently. It was found that roughly 2.5 hours is the best amount of time. We determined that ion concentration made very little difference by excluding ions from the sample, or the wash buffer and then having them present in both as a control. The focus then fell upon the elution buffer, working from the original papers we had a much lower sugar concentration in the initial protocol than was necessary. Increasing the ion concentration was attempted at first but to no avail, the salt concentration was then increased again no real difference was noted, finally there was an increase of the sugar concentration from 0.15M, to 0.3M this increased the rhodopsin concentration in the mutants. It should be noted that the amendments to the protocol were all done

using purified ROS rhodopsin meaning that for harvested rhodopsin from cell extracts this protocol may need to altered again.

Figure 16 shows the mutant con A-sepharose wash and elution fractions as well as that of WT. we can clearly see that figure 15.E (WT) has successfully eluted out rhodopsin which means that it is possible to run both separation protocols on a recombinant rhodopsin and get the full rhodopsin eluted. Figure 16 A-D show the mutant rhodopsin, we can see that the washes from each shown in purple appear to drop off at the 280nm mark whereas the elution fractions seem to increase at the 280nm mark. This stark difference could be due to the difference in buffer content and poor blanking. There appears to be no peaks showing at 490nm, we can see this more clearly from figure 17 which shows a zoomed in graph of figure 16. This is due to the low quantities of rhodopsin being tested, in order to show a clear peak, the difference spectra should be shown. The difference spectra however was never measured and the samples were thrown away before this could be rectified. The low volumes of rhodopsin are to be expected after two separation columns.

Figure 17 D seems to show a slight change in the incline of the wash fraction at roughly 490nm. The wash fraction is producing a higher level of absorbance than the elution sample, this could potentially mean there is more rhodopsin present in the wash fraction. Given that the truncated rhodopsin mutant would not bind to the Con A it would be fractioned off either at the flow through or the wash, thus we could be seeing rhodopsin here. This agrees with previous work which found that P23H showed the highest level of truncated species, which could be why this has not been replicated in the other mutants (Krebs, et al., 2010). It should be noted from figure 16. D that there is a dip for the wash at 280nm, which would indicate a lack of protein. It is also possible that due to the changing buffers, the blanks for these washes were not accurate which would have skewed the data.

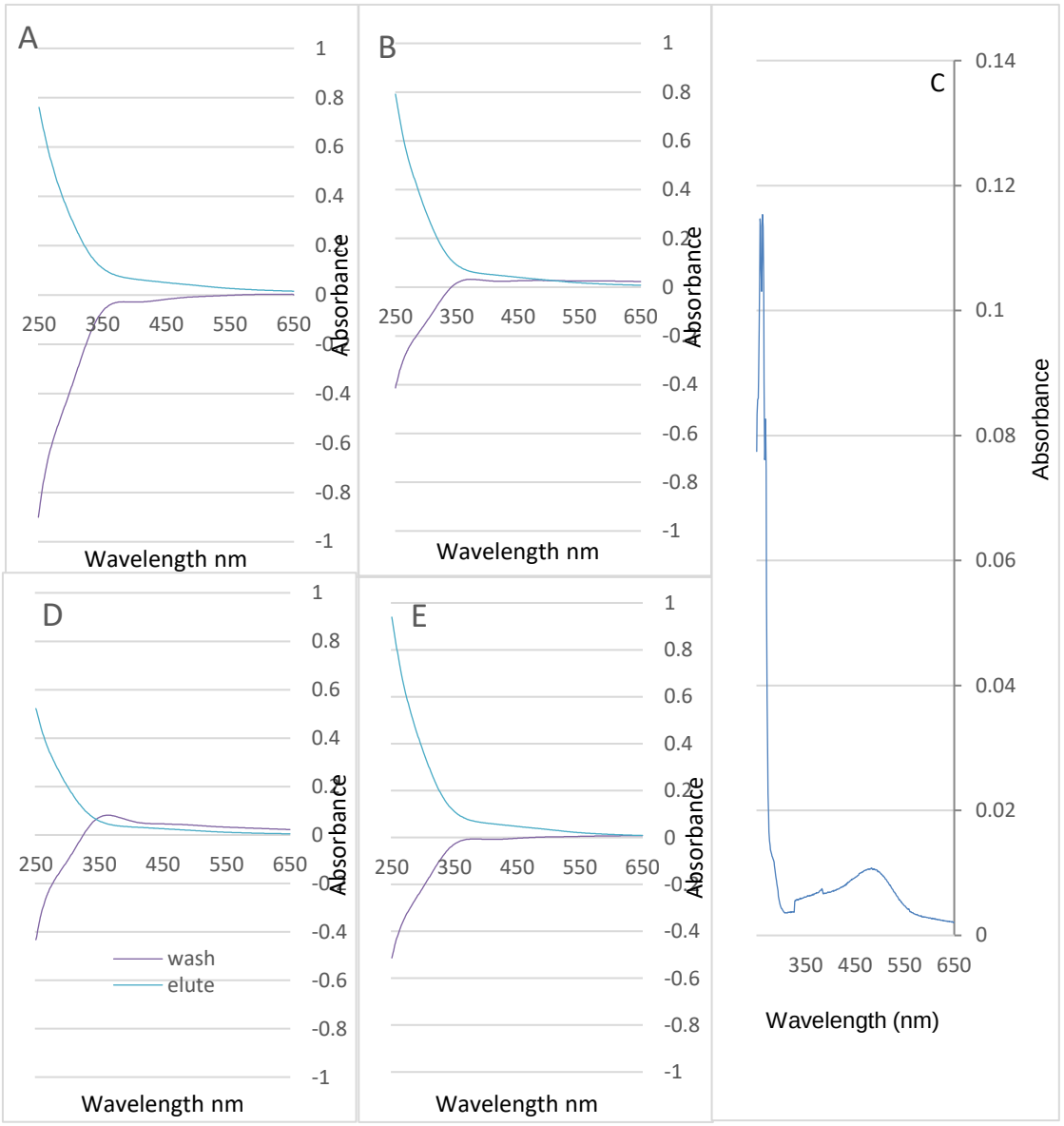

Figure 16 The UV spectra of WT and ADRP rhodopsin obtained from the wash and elution fractions of Con A-Sepharose separation protocol. The samples were first purified using the protocol 1D4-sepharose separation. The samples were then bound to Con A Sepharose beads, subjected to washing before an elution buffer containing Methyl α-D-Mannopyranoside was added which competed with the rhodopsin allowing the full ADRP rhodopsin mutant to be eluted off. The protocol was preformed on the first Elution of 1D4-sepharose separation of ADRP rhodopsin mutants seen in Figure 14 and 15. The mutants are in the following order; A – Q28H , B-P23A, c WT D- P23H E- T4K.

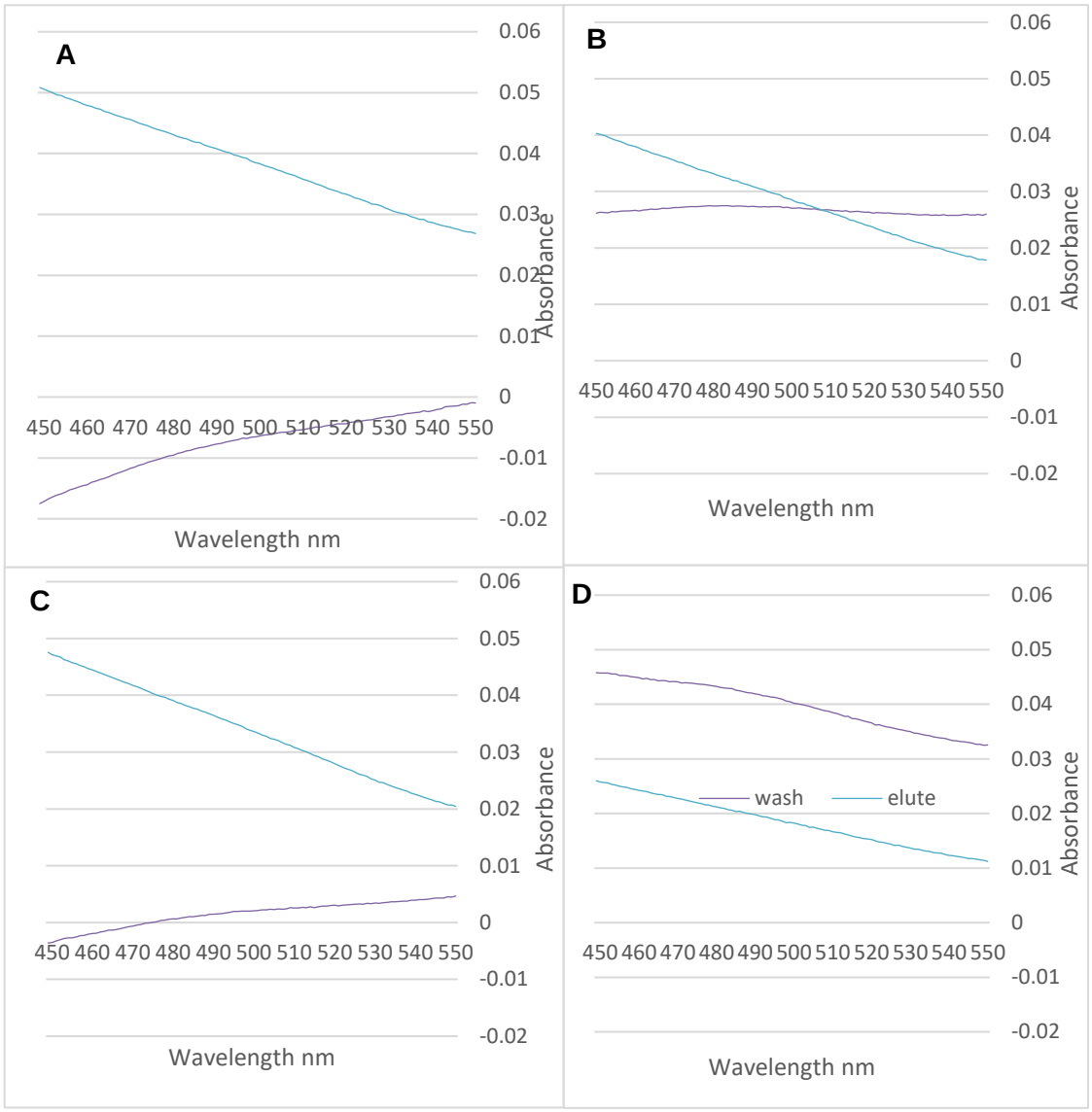

Figure 17 The UV spectra of ADRP rhodopsin obtained from the wash and elution fractions of Con A-Sepharose separation protocol. The samples were first purified using the protocol 1D4-sepharose separation. The samples were then bound to Con A Sepharose beads, subjected to washing before an elution buffer containing Methyl α-D-Mannopyranoside was added which competed with the rhodopsin allowing the full ADRP rhodopsin mutant to be eluted off. The protocol was preformed on the first Elution of 1D4 sepharose separation of ADRP rhodopsin mutants seen in Figure 14 and 15. The mutants are in the following order; A – Q28H , B-P23A, C-T4K D- P23H.

Figure 18 shows the western blot analysis of the separation protocols of P23A against WT separation protocols. We expect that from the 1D4 protocol that we will see minimal rhodopsin present in the wash sample, minimal rhodopsin in after binding sample and high intensity bands showing in the first elution of 1D4 becoming less intense for the second elution. From figure 18 we do see similar results to what we expected. The bands for the first elution are more intense than that seen in the second elution and more intense than the wash and binding samples. We do see rhodopsin present in the binding sample, this means that the rhodopsin in the sample had not fully bound. This could be due as previously stated to low concentrations of 1D4-sephraose beads or low binding time. The rhodopsin is also coming through in the wash albeit showing less intense bands, this again is due to binding issues. The most important point to notice is the lower band, which is showing clearly in the first elution, this means that we are continuing to isolate both the full mutated rhodopsin and the truncated species. We can see this lower band depicting the truncated species in all the elution fractions but not in the wash or binding. The elution fractions show a very clear decrease in intensity of the bands directly reflecting the lower concentration of rhodopsin eluted as we continue through the separation.

From the Con A-sepharose separation we expected to see clear bands showing the truncated species in the after bind and wash samples, we expected to have high intensity bands for rhodopsin in the elution with no band for the truncated species present. In figure 18 we can see P23A original sample has a clear 40kDa band for rhodopsin and lower bands indicating the presence of the truncated form. After binding 1D4 and wash 1D4 do not show the 28kDa band meaning there is no truncated rhodopsin present. There are bands at 40kD showing full mutated rhodopsin indicating loss of rhodopsin throughout binding. This could be due to not enough time being left for the binding or the binding environment was wrong. Full P23A rhodopsin was eluted off, showing that it is possible to separate the rhodopsin mutants in this manner, there

is also an increase in the intensity of the bands for the elution compared with those of the was and after binding flow through, meaning that majority of rhodopsin was bound and eluted as intended.

This protocol requires cold temperatures and no light exposure to ensure that the mutants are well maintained. When repeating this experiment more measures such as air con should be utilised to control these variables. The separation also requires an increase in rhodopsin concentrations, this means increasing concentration at the 1D4-sepharose separation so that this filters down. The binding efficiency of Con A to mutated rhodopsin should be increased, this can be done by testing the environment of the solubilisation buffer and the binding times. This protocol was improved using purified ROS rhodopsin and didn't take into account the contaminates and reduced stability of the rhodopsin mutants. This will need to be adjusted in order to isolate the P23A truncated species.

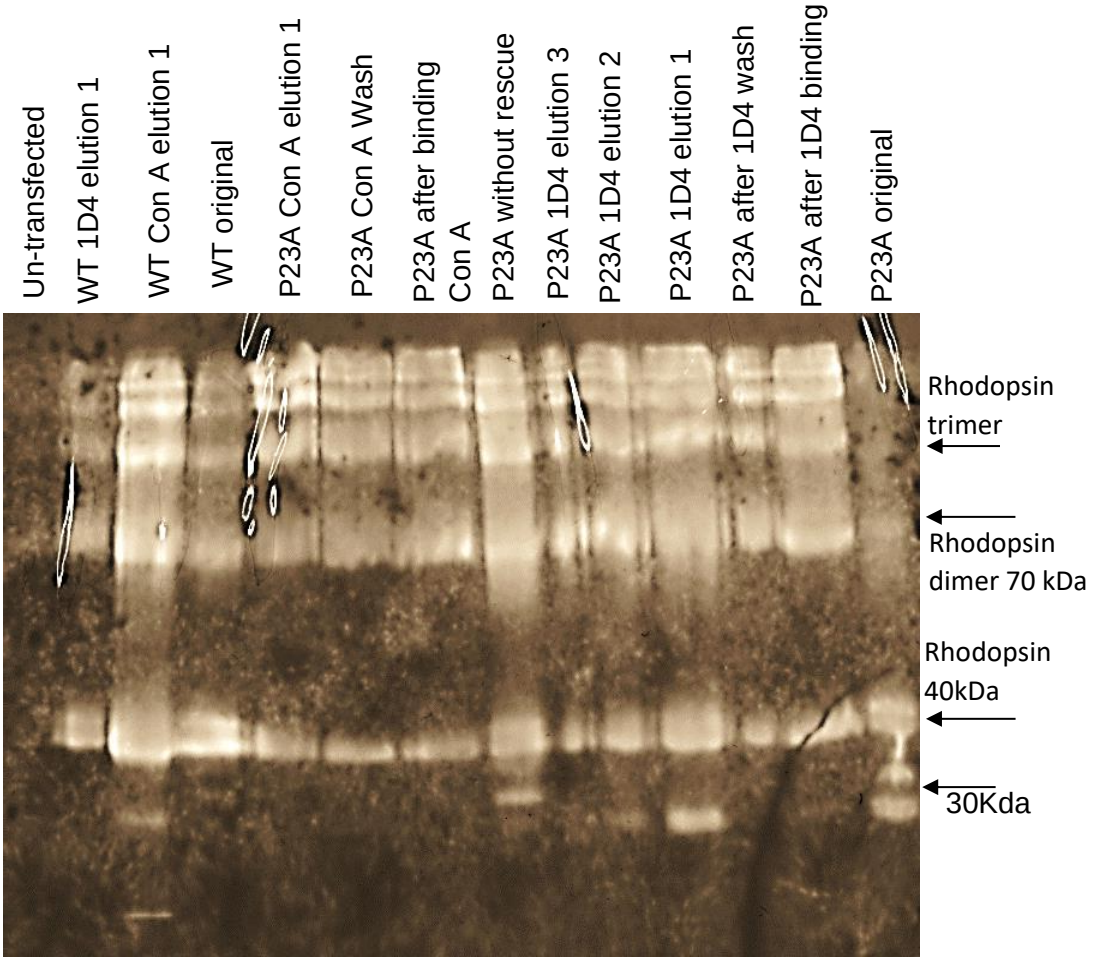

Figure 18 A western blot of the bindings, washes and elutions of both the 1D4 -sepharose separation and the con A-sepharose separation. The

each aims to separate out the rhodopsin by binding either to the C terminus or the N terminus of rhodopsin. Each of the separation protocols and the mutant used is clearly shown at the top. The trimer, dimer and monomer band for rhodopsin is clearly indicated. The lower bands are likely to indicate the truncated rhodopsin.

Future work

Our aim was to increase knowledge of the pathology of retinitis pigmentosa caused by ADRP mutations with the intention of opening pathways for new treatments. We were successful in the first part of our experiments; finding a way to isolate the ADRP truncated species. We proved it is possible to obtain a reasonable amount of rhodopsin after two separation columns using the purified ROS rhodopsin and obtain full P23A rhodopsin after two separation columns. There remain some issues with isolating the truncated species of P23A rhodopsin, which could be for several reasons and modification of the Con A-sepharose immunoaffinity column is needed. The ability to isolate both full and truncated mutated rhodopsin species will enable others to start testing on these separated truncated species to better understand the disease we are fighting.

To prefect the Con A-Sepharose column, the experiment will need to be repeated using higher quantities of ADRP rhodopsin, which will enable us to ascertain whether there was simply was not enough of the truncated species present to show on the western blot. The Con A to rhodopsin ratio will need to be adjusted given that rhodopsin is present in the wash, meaning that not all the rhodopsin was bound to Con A. This means that any separated truncated species will be contaminated.

Having isolated the truncated form of rhodopsin we must now look at its biochemical characterisations, effecting experiments to discover its; thermal stability, photobleaching properties, and metarhodopsin II decay formation. Investigations into these characterisations have all been previously run to compare the outcomes of ADPR mutations to those of the WT, to ascertain the degree of misfolding. In previous papers it has been found that ADRP mutations have behaved unexpectedly in these experiments. The Metarhodopsin II decay kinetics of ADRP mutants were found to be made of both fast and slow components compared with the single component of WT. I expect that re-running these experiments (having isolated the truncated species) will

shed more light on why this is. I would propose running in parallel experiments with WT, the truncated ADRP species, and the full ADRP species, of each mutation.

The natural progression would be to ascertain which of the protein kinases is likely to have caused the truncation of the ADPR mutants. We can select likely kinase inhibitors and test them in batches, running western blot analysis to determine the lack of the lower band located at 28Kda. The rhodopsin harvested will need to undergo biochemical characterisation to learn the degree of misfolding and then to compare this to WT rhodopsin, and the mutated rhodopsin, without kinase inhibitor involvement. This permit understanding of the decrease or increase of stability that is offered by blocking the truncation of the N terminus. If the stability is reaching that of the WT rhodopsin we can consider this a route to possible future treatments for retinitis pigmentosa.

Conclusion

Our aim was to increase understanding of the pathology of retinitis pigmentosa caused by autosomal dominant mutations located in the N terminus. We planned to do this by separating the truncated species of the ADRP mutated rhodopsin from the full species of ADRP mutated rhodopsin using two forms of immunoaffinity chromatography. These are Rho-1D4-sepharose which binds to the TETSQVAPA sequence on the C terminus, and Con A – Sepharose which binds to the glycan moieties located on the N terminus. The truncation removes the glycosylation sites and thus the ability of the truncated species to bind to Con A. The intention was to preform biochemical characterization, preforming experiments on, thermal stability, metarhodopsin II decay, and photobleaching properties.

We managed to obtain high concentrations of ADRP rhodopsin from transient transfection with 9-*cis*-retinal rescue. The results of these confirmed the degree of misfolding found in previous papers. Figure 8 showing P23A to have the highest concentration of rhodopsin, and one of the highest purity ratios. The purity ratio is an approximate reflection of the degree of misfolding. Further to this, and confirming previous work, T4K and P23A continued to show similar purity ratios throughout the experiments, meaning they have a similar degree of misfolding (Krebs, et al., 2010) (Opefi, et al., 2013). We found one outlier in Q28H which consistently had a higher purity ratio, and concentration levels that matched those of P23A. We believe this anomaly is due to the quality of the DNA used at transfection being higher than that of any of the other three mutants, which all behaved as expected.

The 1D4-sepharose separation performed well. We managed to elute rhodopsin from each of the four ADRP rhodopsin mutants. We also greatly increased the purity ratio. Samples in figure 8 produced the following ratios; 0.07 Q28H, 0.05 T4k, 0.05 P23A, and 0.004 P23H, compared favourably with the outcome of the separation protocol in

figure 14, which produced the following; 0.36 Q28H, 0.26 P23A, 0.24 T4k, and 0.17 P23H, showing a marked difference with the Q28H purity ratio increasing five fold.

The Con A sepharose separations however delivered varied results. Figure 13, depicting the Con A – sepharose separation of purified ROS rhodopsin, shows clear peaks at 500 nm for the elution fractions, with just over 70% of rhodopsin eluted in the first elution. This means we created a successful protocol isolating rhodopsin using Con A-sepharose. Figure 17 and 16 do not show clear peaks located at 490nm, which leads to the assumption that no rhodopsin protein was present. The difference spectra is likely to show a much clearer peak at 490nm, however the bleached spectra was not taken and could not be taken as the samples had already been discardedy. If the experiment was to be repeated it would be necessary to obtain the difference spectra to help identify the rhodopsin peaks of these samples. The current lack of peaks in figure 16 and 17 is due to low levels of rhodopsin as would be expected in the event of a secondary separation column. Poor starting concentrations were also instrumental in the inability to identify peaks; having gone through two separation protocols some of the protein was lost in various phases and thus lowered the final concentration of rhodopsin yielded. Figure 18 shows we managed to isolate full P23A rhodopsin but were unable to isolate the P23A truncated species. The band for full P23A rhodopsin, 40kDa, was present in the “wash”, and “after binding” lanes of Con A separation, this means that if the truncated species had been present it would not have isolated. This is due to the poor binding of the P23A mutated rhodopsin to Con A. To increase this binding, further experiments will be needed. These will include investigating the effect of changing, the binding buffer, the concentration of Con A Sepharose, and the binding time. The different outcome of the protocol despite good results form the purified ROS rhodopsin, is likely due to the instability of the mutant. Finally we should mention that it is possible that Con A binding to the mutated rhodopsin differs from that of the WT rhodopsin due to the fact that Con A binds to the glycan moieties located at the

glycosylation sites and these N terminal mutations have been shown to effect the glycosylation sites. However, it is important to note that there is clearly binding of the mutant occurring or the rhodopsin would not have appeared in all the samples, if the protein had not bound it would have washed through prior to the elution.

As with much research multiple complications meant that we were not able to achieve the totality of our original aim, which was to separate the species of mutated rhodopsin, to enable their biochemical characterisation and thus further understanding of retinitis pigmentosa. The research was not without success for instance we managed to separate out the fully formed rhodopsin and our results clearly indicate that it is possible to obtain a truncated form of rhodopsin.

Appendix

1.1 Western blots and SDS page Analysis

Media preparation

4x running buffer

- 18.5g Tris- HCL ph8.8
- 100ml RO water
- Filter sterilised, kept dark at 4°C

4X stacking buffer

- 3g Tris- HCL pH6.8
- 50ml RO water
- Filter sterilised, kept dark at 4°C

1 X Tank buffer

- 0.251M Tris
- 0.192 M glycine
- 0.1% SDS
- Made up in RO water

4X Loading buffer

- 0.25M Tris-HCL (ph 6.8)
- 8% SDS
- 40% Glycerol
- 0.4M DTT
- 0.04% bromophenol blue

1X Transfer buffer

- 0.25M Tris-HCL

- 0.192M Glycine
- 0.1% SDS
- 20% Methanol
- Made up in Ro water

Blocking Buffer

- 10% skim powdered milk
- 0.1% Tween -20 (sigma P-5927)
- 0.1% NaN_3
- Made up in 1X PBS

Wash Buffer

- 0.5% Skim powered milk
- 0.1% Triton X-100(sigma-x100)
- Made up in 1XPBS

ECL

- 10ml of 0.1M Tris-HCL
- 50µl of 0.25M Luminol (sigma 09253)
- 22µl of 0.1M coumaric acid (sigma C-9008)
- 3µL of 30% H_20_2

Primary antibody

- 0.5% gwlatine (sigma G8150 type A)
- 0.25% BSA (sigma 85040-C)
- 0.1M K-Po_4 –Ph 7.4
- 10µg/ml 1D4 antibody
-

Table 1) The procedure for making Running/resolving gel for use in Western blots and SDS page analysis	
Reagents	10% (0.75mm) gel
Acrylamide/Bis-acrymlamide, 30% solution	2.65ml
4X running gel buffer	2.0 ml
10% SDS	0.08 ml
MiliQ water	3.2 ml
10% ammonium persulfate (APS) fresh on the day	0.08ml
*TEMED	0.004ml
Final volume	8 ml

Table 2) The procedure for making Stacking gel for use in Western blots and SDS page analysis	
Reagents	Amont for 4.5ml volume
Acrylamide/Bis-acrymlamide, 30% solution	0.7 ml
4X running gel buffer	1.13 ml
10% SDS	0.06 ml
MiliQ water	2.7 ml
10% ammonium persulfate (APS) fresh on the day	0.06ml
*TEMED	0.004ml
Final volume	4.5 ml

1.12UV spectroscopy

Buffer A – Solubilisation buffer

1% DDM

0.5mM PMSF

In PBS

1.2 Dot blots

Buffer A – Solubilisation buffer

1% DDM

Made up in 1x PBS

Buffer B – Dilution solution

0.1% DDM

1x PBS

Buffer C – wash buffer

(Buffer B + 10x triton)

Buffer D – Blocking Buffer

10% Skim Powdered Milk

0.1% Tween 20 Made up in 1x PBS

0.1% NaN_3

Bibliography

Athanasiou, D., Aguila, M., Bellingham, J., Kanuga, N., Adamson, P., Cheetham, M. E., 2017. The molecular and cellular basis of rhodopsin retinitis pigmentosa reveals potential strategies for therapy. *Progress in retinal and eye research,*62, 1-23.

Baumgartner, W. A., 1999. Etiology, pathogenesis and experimental treatment of retinitis pigmentosa. *Medical Hypotheses,* 54(5), 814-824.

Behnen, P., Felline, A., Comitato, A., Di Salvo, M.T., Raimondi, F., Gulati, S., Kahremany, S., Palczewski, K., Marigo, V., Fanelli. F., 2018. A Small Chaperone Improves Folding and Routing of rhodopsin mutants linked to inherited blindness. *Iscience ,*4, 1-19.

Berson, E. L., Rosner, B., Weigel-DiFranco, C., Dryja, T.P., Sandberg, M. A., 2002. Disease progression in patients with dominant retinitis pigmentosa and rhodopsin mutations. *Investigative ophthalmology and visual science ,* 43(9), 3027-3036.

Blank, T., Goldman, T., Mirja, K., Amann, L., Schon, C., Bonin, M., Pang, S., Prinz, Marco., Burnet, M., Wagner, J. E., Biel, M., Michalakis, S., 2018. Early Microglia activation precedes photoreceptor degeneration in a mouse model of CNGB1-linked retinitis pigmentosa. *Frontiers in immunology,* 8,1930, https://doi.org/10.3389/fimmu.2017.01930.

Bourne, H. R., Meng, E. C., 2000. Rhodopsin sees the light. *Science,* 289(5480), 733-734.

Cha, K., Reeves, P. J. & Khorana, G., 2000. structure and function in rhodopsin: Destabilization of rhodopsin by the binding of an antibody at the N-terminal segment provides support for involvement of the latter in an intradiscal tertiary structure. *PNAS,* 97(7), 3016-3021.

Chen, Y., Chen, Y., Jastrzebska, B., Cao, P., Zhang, J., Wang, B., Sun, W., Yuan, Y., Feng, Z., Palczewski, K. 2014. Inherent Instability of the retinitis pigmentosa P23H mutant opsin. *Journal biological chemistry,* Volume 289, 9288-9303.

Colombo, L., Montesano, G., Sala, B., Patelli, F., Maltese, P., Abeshi, A., Bertelli, M., Rossetti, L., 2018. Comaprison of 5-year progression of retinitis pigmentosa involving the posterior pole among siblings by means of SD-OCT: a retrospective study. *BMC ophthalmology,* 18(1), 1-18.

Comitato, A., Di Salvo, M. T., Turchiano, G., Montanari, M., Sakami, S., Palczewski, K., Marigo, V., 2016. Dominant and recessive mutations in rhodopsin activate different cell death pathways. *Human Molecular genetics,* 25(3), 2801-2812.

Cox, M. M. & Nelson, D. L., 2013. *Lehninger Principles of biochemistry.* 6th ed. New york : W. H. Freeman.

Daiger, S., Sullivan, L. & Browne, S., 2013. Genes and mutations causing retinitis pigmentosa. *Health research alliance,* 84(2), 132-141.

Donders, F., 1857. Beiträge zur pathologischen Anatomie des Auges. *Graefe's Archive for clinical and experimental ophthalmology ,* 3(1857), 139-165.

Fisher, T., 2019. *GeneJet Plasmid Midiprep Kit.* [Online]
Available at: https://www.thermofisher.com/order/catalog/product/K0481#/K0481
[Accessed 18 09 2019].

Fisher, T., 2019. *GeneJet Plasmid Miniprep Kit.* [Online]
Available at: https://www.thermofisher.com/order/catalog/product/K0502#/K0502
[Accessed 12 09 2019].

Fukuda, M. N., Papermaster, D. S., Hargrave. P.A., 1979. Rhodopsin carbohydrate. Structure of small oligosaccharides attached at two sites near the NH2. *Journal of biological chemistry,* 10(253), 8201- 8207.

Fu, Y., 2018. *Phototransduction in rod and cones.* [Online]
Available at: https://webvision.med.utah.edu/book/part-v-phototransduction-in-rods-and-cones/phototransduction-in-rods-and-cones/
[Accessed 12 09 2019].

Hamel, C., 2006. Retinitis Pigmentosa. *Orphanet Journal of Rare Diseases,* 1, 40, https://doi.org/10.1186/1750-1172-1-40.

Hamel, C., 2014. *Orpha net ; Retinitis pigmentosa.* [Online]
Available at: https://www.orpha.net/consor/cgi-bin/OC_Exp.php?Expert=791
[Accessed 24 06 2019].

Hargreave, P. A., 2001. Rhodopsin Structure, Function and Topography The Friedenwald Lecture. *Investigative Ophthalmology and Visual science,* 42(1), 3-9.

Hartlong, D. T., Berson, E. L. & Dryja, T. P., 2006. Retinitis Pigmentosa. *The Lancet,* 368(9549), 1795-1809.

Hofmann, K. P., Scheerar, P., Hildebrand, P.. W., Che, H., Park, J. H., Heck, M., Ernst, O. P., 2009. A G protein-coupled receptor at work: the rhodopsin model. *Trends in Biochemical Sciences ,* 34(11), 540-552.

Hubel, D., 2009. *Eye, Brain and Vision.* 2nd ed. Boston: Harvard medical school.

Kevany, B. & Pakczewski, K., 2012. Phagocytosis of retinal rod and cone photoreceptors. *Physiology ,* 25(1), 8-15.

Khorana, G. H., 1992. Rhodopsin, Photoreceptor of the rod cell : an emerging pattern for structure and function. *Journal of Biological Chemistry,* 267(1), 1-4.

Krebs, M. P., Holden, D.C., Joshi, P., Clark, C.L., Lee, A.H., Kaushal, S., 2010. Molecular mechanisms of rhodopsin retinitis pigmentosa and the efficacy of pharacological rescue. *Journal of Molecular Biology,* 395(5), 1063-1078.

Kusnetzow, A. K., Altenbach, C. & Hubbell, W. L., 2006. Conformational States and Dynamics of Rhodopsin in Micelles and Bilayers. *Journal of Biochemistry,* 45(17), 5538-5550.

Li, S., Mitchell, J., Briggs, D.J., Young, J.k., Long, S.S., Fuerst, P.G., 2016. Morphological Diversity of the Rod Spherule: A study of serially Reconstructed Electron Micrographs. *PLOS,* 11(3), e0150024, doi: 10.1371/journal.pone.0150024.

Lomonosova, E., Kolesnikov, A. V., Kefalov, V. j. & Kisselev, O. G., 2012. Signaling states of rhodopsin in rod disk membranes lacking transducin βγ-Complex. *Investigative ophthalmology and visual science ,* 53(3), 1225-1233.

Marin, E. P., Krishna, A.G., Zvyaga, T.A., Isele, J., Siebert, F., Sakmar, T.P., 2000. The amino terminus of the fourth cytoplasmic loop of Rhodopsin Modulates rhodopsin-transducin interaction. *Journal of Biological chemistry,* Volume 275(3), 1930-1936.

Masland, R. H., 2001. The fundamental plan of the retina. *Nature Neuroscience,* 4(9), 877-886.

Masland, R. M., 2012. The neuronal organization of the retina. *Neuron,* 76(2), 266-280.

Mcdevitt, D., 2012. *Cell Biology of the eye.* 1st ed. London: Academic Press.

Mendes, H. F., Van der Spuy, J., chapple, J. P. & Cheetham, M. E., 2005. Mechanisms of cell death in rhodopsin retinitis pigmentosa: implications for therapy. *Trends in Molecular Medicine ,* 11(4), 177-185.

Molday, R. s. & Moritz, O. L., 2015. Photoreceptors at a glance. *Journal of cell Science,* 128(22), 4039-4045.

Na, K., Kim, H.J., Kim, K.H., Han, S., Kim, P., Hann, H.J., Ahn, H.S., 2017. Prevalence, Age at Diagnosis, Mortality, and cause of death in retinitis pigmentosa in

Korea - A nationwide population-based study. *American Journal of Ophthalmology* ,176, 157- 165.

Natarajan, S., 2011. Retinitis pigmentosa: A breif overview. *Indian Journal of Opthalmology,* 59(5), 343-346.

Nemet, I., Ropelewski, P. & Imanishi, Y., 2015. Rhodopsin trafficking and Mistrafficking. *Progress in Molecular Biology and Translational science,* 132, 39-71.

Ogata, S., Muramatsu, T. & Kobata, A., 1975. Fractionation of Glycopeptides by Affinity Column Chromatography on Concanavalin A-sepharose. *Journal of Biochmistry,* 78, 687-698.

O'Neill, J., McKay, G., Smipson, D. & Silvestri, G., 2007. The Epidemiology of retinitis pigmentosa in Northen Ireland. *Investigative Ophthalmology and visual science ,* 48(13), 3724

Opefi, C. A., South, K., Reynolds, C.A., Smith, S.O., Reeves, P.J, 2013. Retinitis Pigmentosa mutants provide insight into the role of the N-terminal cap in rhodopsin folding, stucture, and function. *Biological Chemistry,* 288(47), 33912-33926.

Palczewski, K., Kumasaka, T., Hori, T., Behnke, C.A., Motoshima, H., Fox, B.A., Trong., L.I., Teller, D.C., Okada, T., Stenkamp, R.E., Yamamoto, M., Miyano, M., 2000. Crystal structure of rhodopsin: A G protein-coupled receptor. *Science,* 289(5480), 739-745.

Price, B. A., Sandocal, I.M., Chan, F., Simons, D. L., Wu, S. M., Wensel, T. G., Wilson, J. H., 2011. Mislocalization and degradation of Human P23H-rhodopsin-GFP in a knockin Mouse Model of retinitis pigmentosa. *Invest Ophthalmol Vis Sci,* 52(13), 9728-9736.

Rakoczy, E. P., Kiel, C., McKeone, R., Stricher, F., Serrano, L., 2011. Analysis of Disease-Linked Rhodopsin Mutations Based on Structure, Function and protein stability calculations. *Journal of molecular biology,* 405(2), 584-606.

Ramon, E., Cordomí, A., Aguilà, M., Srinivasan, S., Dong, X., Moore, A. T., Webster, A.R., Cheetham, M.E., Garriga, P., 2014. Differential light-induced responses in sectorail inherited retinal degeneration. *The Journal of Biological Chemistry ,* 289(52), 35918-35928.

Rathnasamy, G., Foulds, W. S., Ling, E.-A. & Kaur, C., 2018. Retinal Microglia – a Key Player in Healthy and diseased Retina. *progress in neurobiology,*173, 18-40.

Ravichandran, G., Elangovan, P. & Nath, M., 2019. Diagnosis of retinitis pigmentosa from retinal images. *INTL journal of electronics and telecommunications ,* 65(3), 519-525.

Reeves, P. J., Callewaert, N., contreras, r. & khorana, G. H., 2002. Structure and function in rhodopsin: high-level expression of rhodopsin with restricted and homogeneous N-acetylglucosaminyltransferase l-negative HEK293s stable mamalian cells. *PNAS,* 99(21), 13419-13424.

Reeves, P., Kim, J.-m. & Khorana, G. H., 2002. Strucuture and function in rhopsin: A tetracycline-inducible system in stable mammalian cell lines for high-level expression of opsin mutants. *PNAS,* 99(21), 13413-13418.

Reminington, L. A., 2011. *Clinical Anatomy and physiology of the visual system.* 3rd ed. st louis: Elsevier; Butterworth-Heinmann.

Rivolta, C., Sharon, D., DeAngelis, M. M. & Dryja, T. P., 2002. Retinitis pigmentosa and allied diseases: numerous diseases, gene, and inheritance patterns. *Human Molecular Genetics,* 11(10), 1219-1227.

Sakami, S., Maeda, T., Bereta, G., Okano, K., Golczak, M., Sumaroka, A., Roman, A. J., Cideciyan, A.V., Jacobson, S.G., Palczewski, K., 2011. Probing mechanisms of photoreceptor degeneration in a new mouse model of the common form of autosomal dominant retinitis pigmentosa due to P23H opsin mutations. *Journal of biological Chemistry,* 286, 10551-10567.

Schultz, C., 2013. *Newly Approved Retinal Implants can help blind people see.* [Online]
Available at: https://www.smithsonianmag.com/smart-news/newly-approved-retinal-implants-can-help-blind-people-see-18983874/
[Accessed 18 09 2019].

Life Maps Discovery, 2019. *The cellular structure of the retina.* [Online] Available at: https://discovery.lifemapsc.com/library/images/the-cellular-structure-of-the-retina
[Accessed 13 07 2019].

Thermo Scientific., 2019 *Overview affinity chromatography.* [Online]
Available at: https://www.thermofisher.com/es/es/home/life-science/protein-biology/protein-biology-learning-center/protein-biology-resource-library/pierce-protein-methods/overview-affinity-purification.html
[Accessed 13 05 2019].

Sekharan, S., Morokuma, K., 2011. Why 11-*cis*-Retinal? Why Not 7-*cis*, 9-*cis* or 13-*cis*-Retinal in the Eye? *Journal of the American Chemical Society,* 133(47), 19052-19055.

Shichi, H., Adams, A. & Kobata, A., 1980. The oligosaccharide moiety of rhodopsin - its structure and cellular location. *Neurochemistry International,* 1, 245-253.

Snell, R. S. & Lemp, M. A., 1998. *Clinical anatomy of the eye.* 2nd ed. Malden. MA: Blackwell science.

Strauss, O., 2005. The retinal pigment epithelium in visual function. *physiological reiews,* 85(3), 845-881.

Sung, C. & Chuang, J., 2010. The cell biology of Vision. *Journal of cell biology,* 190(6), 953-963.

Tam, B. M. & Moritz, O., 2007. Dark Rearing Rescues P23H Rhodopsin-Induced Retinal Degeneration in a transgenic Xenopus Laevis Model of retinitis Pigmentosa: A Chromophore-Depenednent Mechanism Characterized by Production of N-

terminally Truncated Mutant Rhodopsin. *Journal of Neuroscience ,* 27(34), 9043-9053.

Tam, B. M. & Moritz, O. L., 2007. Dark Rearing Rescues P23H Rhodopsin-Induced Retinal Degeneration in a Transgenic Xenopus laevis Model of Retinitis Pigmentosa: A Chromophore-Dependent Mechanism Characterized by Production of N-Terminally Truncated Mutant Rhodopsin. *Journal of Neuroscience ,* 27(34), 9043-9054.

Tam, B. M., Noorwez, S.M., Kaushal, S., Kono, M., Mortiz, O., 2014. Photoactivation-Induced Instability of Rhodopsin Mutants T4K and T17M in Rod Outer Segments Underlies Retinal Degeneration in X. laevis Transgenic Models of Retinitis Pigmentosa. *Journal of neuroscience,* 24(40), 13336-13348.

Thoreson, W. B., Babai, N. & Bartoletti, T. M., 2008. Feedback from horizontal cells to rods photoreceptors in vertebrate retina. *Journal of Neuroscience ,* 28(22), 5691-5695.

Tsukamoto, H. & Terakita, A., 2010. Diversity and functional properties of bistable pigments. *Photochemical and photobiological sciences,* 9(11), 1435-1443.

Verbakel, S. K., Van Huet., R. A., Hollander, A.I.D., Collin, R.W.J., Klaver, C.C.W., Hoyng, C.B., Roepman, R., Klevering, B.J., 2018. Non-syndromic retinitis pigmentosa. *Progress in retinal and eye research,*66, 157-186.

Vogel, R., Mahalingham, M., Lüdeke, S., Huber, T., Siebert, F., Sakmar, T. P., 2008. Functional role of the "ionic lock"- an interhelical hydrogen bond network in family a heptahelical receptors. *Journal Molecular Biology,* 380(4), 648-655.

William, K. J., 2005. *Krause's Essential Human Histology for Medical students.* 3rd ed. Boca Raton: Uuniversal Publishers.

Zhang, Q., 2016. Retinitis Pigmentosa: progress and perspective. *The Asia-Pacific Journal of Opthalmology,* 5(4), 265-271.

Zhou, E. X., Melcher, K. & Xu, E., 2012. Strcuture and activation of rhodopsin. *Acta pharmacologica sinica,* 33(3), 291-299.